How is rockfall risk impacted by land-use and land-cover changes? Insights from the French Alps

Manon Farvacque, Jérôme Lopez-Saez, Christophe Corona, David Toe, Franck Bourrier, Nicolas Eckert

▶ **To cite this version:**

Manon Farvacque, Jérôme Lopez-Saez, Christophe Corona, David Toe, Franck Bourrier, et al.. How is rockfall risk impacted by land-use and land-cover changes? Insights from the French Alps. Global and Planetary Change, 2019, 174, pp.138-152. 10.1016/j.gloplacha.2019.01.009 . hal-01994621

HAL Id: hal-01994621
https://hal.science/hal-01994621

Submitted on 21 Oct 2021

HAL is a multi-disciplinary open access archive for the deposit and dissemination of scientific research documents, whether they are published or not. The documents may come from teaching and research institutions in France or abroad, or from public or private research centers.

L'archive ouverte pluridisciplinaire **HAL**, est destinée au dépôt et à la diffusion de documents scientifiques de niveau recherche, publiés ou non, émanant des établissements d'enseignement et de recherche français ou étrangers, des laboratoires publics ou privés.

Distributed under a Creative Commons Attribution - NonCommercial 4.0 International License

Version of Record: https://www.sciencedirect.com/science/article/pii/S092181811830314X
Manuscript_6202e428d5b8007deafb750d7f18e32e

How is rockfall risk impacted by land-use and land-cover changes? Insights from the French Alps.

Manon Farvacque [a], Jérôme Lopez-Saez [b], Christophe Corona [c], David Toe [d], Franck Bourrier [d], Nicolas Eckert [a]

[a] Univ. Grenoble Alpes, Irstea, ETNA, 38000 Grenoble, France.

[b] Climate Change Impacts and Risks in the Anthropocene, Institute for Environmental Sciences, University of Geneva, 66 Boulevard Carl Vogt - 1205 Geneva, Switzerland.

[c] Université Clermont Auvergne, CNRS, GEOLAB – 63000 Clermont-Ferrand, France.

[d] Univ. Grenoble Alpes, Irstea, LESSEM, 38000 Grenoble, France.

Abstract

Due to intense urban sprawl in rockfall-prone areas, a precise rockfall risk assessment has become a crucial issue for public authorities and stakeholders. In this context, quantitative risk analysis (QRA) procedures, accounting for the specificities of the rockfall process, have been developed. For the last few decades, several studies have examined the impacts of global warming on rockfall activity, especially at high-altitude sites. However, the influence of land-use and land-cover (LULC) changes, very frequent at lower altitudes and in the vicinity of urbanised areas, on rockfall propagation and associated risks has received little attention.

This study proposes a holistic QRA on a municipality scale (the municipality of Crolles, in the French Alps) that includes both all the potential release areas at the whole cliff scale and a wide spectrum of rockfall volumes randomly extracted from volume classes distributed between 1 and 20 m^3. In addition, to quantify precisely the effect of LULC changes on rockfall risk, four characteristic scenarios representative of LULC changes observed in the municipality and more generally in the Alps since the mid-19^{th} century, have been included in the analysis.

The results demonstrate the significant impacts of landscape reorganisation on the spatial distribution of risk with increasing forest cover, which can be counterbalanced by evolving LULC in a transition unit located between the forest strip and the urban front. They also evidence that a large proportion of the risk is explained by small block volumes, which are the most affected by landscape structure and evolution. From a practical point of view, and despite several uncertainties related to different modelling assumptions, the results reported herein clearly demonstrate the applicability and the value of QRA for rockfall risk management at a municipality scale in a context of rapid and intense environmental changes.

Keywords: Land-use and land-cover changes; Rockfall risk; Quantitative Risk Analysis; Non-stationary process

© 2019 published by Elsevier. This manuscript is made available under the CC BY NC user license
https://creativecommons.org/licenses/by-nc/4.0/

1. Introduction

Rockfalls are widespread phenomena in mountainous regions, described as the free falling, bouncing and/or rolling of individual rocks and boulders of different sizes originating from (sub)vertical cliffs (Varnes, 1978; Erismann and Abele, 2001). They are triggered by multiple factors such as short-term weather conditions (freeze-thaw events, temperature variations or intense precipitation), seismic activity, permafrost degradation, vegetation (root wedging) or human activities (D'Amato et al., 2016; Noetzli, 2003). This multiplicity of triggering factors, the lack of reliable precursor signals, the sudden occurrence of rockfalls as well as individual rock detachment (Hantz, 2013) result in a spatio-temporal unpredictability that endangers human lives, transportation infrastructure, industry and housing. Abundant literature reports fatalities in Alpine environments, e.g., in Switzerland (Badoux et al., 2016; Straub and Schubert, 2008), France (Assali, 2015), Italy (Agliardi et al., 2009) and Austria (Haque et al., 2016). Rockfall protection through rigorous land-use planning based on hazard zoning maps and/or appropriate risk mitigation measures is therefore a crucial issue for authorities and stakeholders in rockfall-prone areas (see e.g. Agliardi et al., 2009; Corominas et al., 2005). Although hazard zoning is a useful tool for land planning, the design and optimisation of both structural and non-structural protective countermeasures require precise risk analysis and evaluation (Volkwein et al., 2011).

In that respect, quantitative risk assessment (QRA) procedures developed for landslides (Corominas et al., 2013; Fell et al., 2005, 2008; Lari et al., 2014) have been adapted to account for the specificities of rockfall processes (Agliardi et al., 2009; Corominas et al., 2013, 2005; Corominas and Mavrouli, 2013; Moos et al., 2017). They classically include each term of the risk components in the form of probabilities and the estimation of probable consequences, so that risk can be expressed in monetary value (Hackl et al., 2018). In addition, in the case of rockfalls, they integrate 3D numerical models to evaluate the spatial probability and intensity of impacts on structures (Agliardi et al., 2009). QRA differs from qualitative risk analysis by the input, the procedures used in the analysis and the final risk output. In contrast with qualitative risk analysis, such as the Rockfall Hazard Rating System (RHRS) (Budetta, 2004; Budetta and Nappi, 2013; Ferrari et al., 2016), which yields results in terms of weighted indices, QRAs quantify the probability of a given level of loss. For society in general, QRAs help increase the awareness of existing risk levels and the appreciation of the efficiency of the actions undertaken (Corominas et al., 2013). However, in practice, the quantitative estimation of the different components of risk is challenging (Corominas et al., 2005) due to the spatially distributed nature of rockfall processes, for which both the probability of an impact on different elements at risk and intensity vary significantly along block trajectories. The challenge

also stems from the detailed data and/or economic resources required for these analyses (Ferrari et al., 2016). As a consequence, the literature focusing on QRAs in rockfall-prone regions remains scarce (see Corominas et al., 2013, for a review). QRAs are mostly site-specific (Ferrari et al., 2016) and restricted to critical release areas with a retro-analysis of rockfalls involving a few blocks (Corominas et al., 2005; Agliardi et al., 2009). In addition, most of these studies only consider a partial distribution of rockfall volumes and do not account for the spectrum of hazard scenarios. More broadly, as for other natural hazards, classical rockfall risk evaluation procedures are defined under stationary conditions, implying that events arise with a constant probability distribution over time. This ignores possible rockfall activity variations related to environmental changes (Eckert et al., 2018). However, over the last few decades mountain zones, where most rockfall risk is located, have experienced strong and rapid socio-environmental mutations combined with the rapidly changing climate (e.g., Beniston et al., 2018). Since the beginning of the last century, in European mountain regions (Kamada and Nakagoshi, 1997; Romero-Calcerrada and Perry, 2004; Walther, 1986), the abandonment of traditional agriculture has produced vegetation succession occurring at varying rates dependent on the site conditions. This process results in dense shrub cover and finally in reforestation (Tasser and Tappeiner, 2002). In the vicinity of urban areas, this rapid agro-pastoral decline has been followed by intense periurban expansion since the mid-20th century. Interactions and retroactions between natural hazard processes, social practices, periurban sprawl and ecosystem changes are numerous (e.g., Field and Intergovernmental Panel on Climate Change, 2012). This results in substantial changes in mountain risks, potentially differing greatly from one area to another (e.g., Stoffel and Huggel, 2012). In the specific case of rockfall, a few studies have documented an increase in high-altitude rockfall frequency related to global warming and permafrost degradation (Einhorn et al., 2015; Noetzli, 2003; Ravanel and Deline, 2011). Yet, to our knowledge, at lower altitudes and within a QRA approach, no study has integrated the evolution of landscape patterns that potentially affect rockfall propagation and energy (Lopez-Saez et al., 2016). This lack of dynamical analyses precludes reliable anticipation of rockfall risk in a context where environmental conditions are evolving rapidly and substantially.

In contrast to previous studies restricted to the retro-analysis of a few critical release areas, we investigated here a complete 3-km-long limestone cliff, located on the edge of the Isère Valley (French Alps), in the municipality of Crolles, where (i) numerous rockfalls, (ii) an intense agro-pastoral decline and (iii) rapid periurbanisation – related to the nearby Grenoble conurbation (500,000 inhabitants) – have been reported since the beginning of the 20th century (Lopez-Saez et al., 2016). To quantify the impacts of land-use and land-cover (LULC) changes on rockfall risk, we (i) determined a volume-frequency relationship for rockfall events at Crolles using an asymptotic model of the generalised Pareto family, which better accounts for the frequency of extreme events than previously used

power-law approaches, through detailed historical/field observations; (ii) performed a quantitative risk analysis simultaneously including all the release areas that potentially threaten the village as well as (iii) the whole distribution of rockfall volumes randomly extracted in the range 1-20 m^3; (iv) adapted a rockfall simulation model to keep track of each simulated individual trajectory; (v) expressed the risk in m^2 destroyed per year at the level of each individual building and (vi) compared the spatial risk distribution, the overall mean annual value at the scale of the entire study area and the risk distribution among 19 equal volume classes for four characteristic LULC patterns observed over the last 150 years at Crolles. These different LULC patterns, associated with the pre-industrial, post-World-War II, urban sprawl and current periods in Crolles, can all still be encountered today on south-facing slopes in the calcareous Alps.

Based on this approach, we propose a holistic QRA procedure where each risk component is precisely quantified. The implementation of the four archetypal landscapes within the analysis contributes to the broader scope of the results providing, for the first time, a risk analysis that takes into consideration non-stationary environmental conditions.

2. Study site

The village of Crolles (45°17′09″N, 5°53′01″E) is located in the Isère department, northeast of the Grenoble conurbation (Fig. 1A, B). It covers an area of 14.2 km^2 from the Bec Margain (1036 m a.s.l.) to the Isère River (220 m a.s.l.) (Fig. 1C). The village is settled on the eastern slope of the Chartreuse Massif (French Alps), with slope angles that decrease gradually from 45-50° in its upper portion to 15° at the level of the urban front with a marked concavity between 300 and 350 m a.s.l. It is topped by a 300-m-high sub-vertical cliff made of thick-bedded limestones and marls from the upper Jurassic period (Dussauge-Peisser et al., 2002). The cliff triggers rockfall with sizes varying from gravel clasts to blocks with volumes greater than 30 m^3. Historical archives, fresh blocks, recent impact craters on the ground and visible growth disturbances (i.e. scars, decapitated trees) on the forest stand confirm ongoing numerous rockfalls released from the entire cliff section. Since the mid-20th century, the village has experienced intense periurban expansion. Several neighbourhoods (Fragnès, Magny, Coteau, Ardillais) have spread over the southeastern slopes of the Chartreuse Massif (Fig. 1C), and are therefore exposed to increasing danger related to rockfall activity. As a consequence, since 1995 several protective walls have been constructed to reduce rockfall risk and an additional 1-km-long dike will soon be finalised (Fig. 1C).

At Crolles, LULC patterns have undergone major changes since 1850 with a clear trend towards an increase in forest cover and urban areas (Fig. 1D, E). In 1850, the slope was characterised by a quasi-binary landscape with (i)

124 vineyards occupying up to 28° slope gradients at altitudes below 450 m a.s.l. where a continuous forest strip then
125 took over to extend up to the base of the calcareous cliff (Fig. 1D). Urban and cultivated allotments are scattered
126 below 280 m a.s.l. but only cover spatially limited surfaces, typically on gentle slopes. For the period between
127 1850 and the 1950s, historical documents evidence a generalised abandonment of vineyards. A similar decline in
128 viticulture has been observed in alpine vineyards between 1880 and the 1970s and is related to (i) the generalised
129 agricultural decline after the First and Second World Wars, (ii) the phylloxera (*Phylloxera vastatrix*) outbreaks that
130 destroyed most vineyards in 1880-1890 (Stevenson, 1980; Veyret-Verner, 1937), (iii) the increasing competition
131 from wines from southeastern France and (iv) the disappearance of the Grenoble military market in 1925
132 (Grandvoinnet, 2011). Schematically speaking, downslope wine plots have been replaced by grasslands. The
133 upslope allotments were abandoned first and were either replaced with untilled land or colonised by the upcoming
134 forest. In the 1980s, the abandonment of agricultural plots and the spread of the forest continued to affect the
135 areas upslope of the main constructed areas. Finally, nowadays the landscape is characterised by a dense forest
136 cover on most of the slope and the presence of discontinuous grassland plots scattered among constructed and
137 wooded plots (see Lopez-Saez et al., 2016, for a detailed description). LULC changes are accompanied by a sharp
138 increase in the length of the urban front potentially exposed to rockfall controlled by the rapid expansion of the
139 Grenoble peri-alpine conurbation (Fig. 1E).
140 In this paper, we deliberately decided to disregard the urban development from our analysis in order to isolate the
141 impacts of landscape dynamics on the rockfall risk. This decision was also supported by the complexity of
142 evaluating exposed structures in the mid-19th century. For the same reasons, the risk calculation does not account
143 for the current protective walls. As a consequence, we decided to use four LULC maps obtained from the
144 diachronic landscape analysis performed in Lopez-Saez et al. (2016) as patterns roughly representing the pre-
145 industrial (hereafter referred to as the binary pattern), post-World-War II (mosaic A pattern), urban sprawl (mosaic
146 B pattern) and current (densely forested pattern) periods (Fig. 2). The urban front exposed to rockfalls was
147 delineated from the cadastral map and included in the quantitative risk analysis for each pattern.
148
149 **3. Risk framework and numerical model set-up**
150
151 3.1 General framework and computation
152

Risk is generally defined as a combination of the damageable phenomenon and its consequences (Eckert et al., 2012), thus describing a statistical value for the expected damage per year. By considering all the scenarios which characterise a risk situation, the rockfall risk can be expressed with the following integral:

$$R_w = \sum_{z \in w} q(z_w)\, z_w \int f(\text{Event})\, p_z(\text{Event})\, D_z(\text{Event}) d\text{Event} \quad (1)$$

R_w represents the expectations of the consequences (or a certain amount of damage) of hazard activity for the whole system at risk, w. This system is composed of a set of any element or combination of elements z potentially at risk, characterised by an exposure factor $q(z_w)$ and a value z_w.

In the most common configurations, these elements are physical (i.e. people, traffic infrastructure, buildings), but other less tangible aspects can be introduced such as the image and aesthetics of an element (Eckert et al., 2012).

The frequency f(Event) of the hazard, the reach probability p_z(Event) on an element at risk z and the resulting damage D_z(Event) are derived for all possible events and are representative of physical and kinetic rockfall properties (i.e. volume, mass, shape, translational and rotational energies, passing height, impact angle, etc.).

Due to the complexity and suddenness of rockfall processes, several parameters that would be useful for risk assessment are systematically lacking (Bourrier et al., 2016; Eckert et al., 2012). A simplified approach in which only rock volumes and kinetic energies are included is generally adopted following the equation:

$$R_w = \sum_{z \in w} q(z_w)\, z_w \int f(v) \left[\int p_z(E|v)\, D_z(E)\, dE \right] dv \quad (2)$$

where f(v) corresponds to the occurrence frequency of rockfall events with a volume v, $p_z(E|v)$ the reach probability on an element at risk z by a block of volume v with an energy E and $D_z(E)$ the resulting damage on z for an impact energy E.

Risk analysis is performed numerically on a case-by-case basis (Fig. 3) by distinguishing each element at risk z identified in the system w. The risk value specific to each element z is approximated by discrete sums on several volume classes. For each of these volume classes, the damaging value is evaluated by the Monte Carlo method as:

$$\overline{D}_z\left(V_{CL_i}\right) \approx \frac{1}{N} \sum_{k=1}^{N} D\,(z, E_k) \quad (3)$$

where $E_k \in [1, N]$ is the local distribution of rockfall energies evaluated over N simulations. Thus, the risk for the element z is expressed as:

$$R_z = q(z_w) \times z_w \times \sum_{i=1}^{l} f(V_{CL_i}) \times p_z(V_{CL_i}) \times \overline{D}_z(V_{CL_i}) \quad (4)$$

where the volume distribution is discretised in V_{CL} classes.

Finally, the total risk for the system w is the sum of individual risks for each of the elements z (Eckert et al., 2012), i.e.:

$$R_w = \sum_{z=1}^{m} R_z \quad (5)$$

3.2 Rockfall probability

In rockfall terminology, the rockfall hazard refers to the probability of an event (rockfall) of a given magnitude (volume) or intensity (energy) over a predefined period of time and within a given area (see e.g. Varnes 1984, Ferrari et al., 2016). This parameter involves both the spatial probability of occurrence (i.e. susceptibility) and the related temporal probability, which is also called the probability of failure (i.e. frequency).

Susceptibility is the likelihood that a block departure event will occur in a specific area based on the local terrain conditions (Brabb, 1984). Previous studies mostly used release points of historical rockfall events or geological/geostructural/geophysical approaches (characterisation of discontinuities and failures, photogrammetry, terrestrial laser scanning, microseismic monitoring; Assali, 2015; Budetta, 2004) to detect and map rock instabilities. These approaches are usable for small-scale sites but are not suitable for larger-scale approaches. Given that gravity is the main driving force acting on slopes and that it is directly proportional to the inclination (Loye et al., 2009), the morphology of a terrain displays characteristic slope angles that can be directly related to morphological units (such as rock cliffs, steep slopes, foot slopes and plains). In this study, we applied a DEM-based geomorphometric approach known as the slope angle frequency distribution (SAFD) procedure (Loye et al., 2009; Michoud et al., 2012) to detect rockfall release areas at the whole-cliff scale. In this procedure, using the Excel-

based Histofit application, slope angle distribution is decomposed in several Gaussian distributions. The terrain is considered a potential rockfall source if its slope angle exceeds a certain threshold, which in turn is defined where the Gaussian distribution of the "rock cliff" morphological unit becomes dominant over the "steep slope" unit.

In addition to susceptibility, the temporal probability of failure must be addressed to define the probability of the occurrence of a rockfall event, expressed in terms of frequencies or return periods (Ferrari et al., 2016). In this study, the temporal probability of a rockfall with a given volume was evaluated through a return rockfall-frequency procedure (De Biagi et al., 2017), which investigates historical events to (i) describe the temporal occurrence of the events and (ii) describe the rockfall volume distribution. For this purpose, 29 blocks with volumes ranging from 0.2 m^3 to 10 m^3 were inventoried along a 900-m-long transect located in the Ardillais neighbourhood (Fig. 1C).

Statistical modelling of extreme values has now emerged as an important statistical discipline that aims at generically quantifying the stochastic behaviour of extreme events (Coles, 2001). Here, by contrast with previous studies where a power-law approach was used (Dussauge-Peisser et al., 2002; Lopez-Saez et al., 2016), we adopted an asymptotic model from the generalised Pareto distribution (GPD) family to characterise the distribution of volumes exceeding a volume threshold value u. According to Pickands (1975), for any random variable, this is the true limiting distribution as soon as u is high enough. In this study, the threshold u = 1 m^3 was used because we consider it the minimum volume that can significantly damage buildings. Finally, a catalogue containing only the volumes u and greater was retained from field observations. Given an estimated observation period evaluated at 100 years (see Results section), this catalogue is used to estimate the temporal occurrence frequency of the events ($\hat{\lambda}$) and the local estimates for the GPD model. The annual cumulative distribution of rockfall volumes (Fig. 4) is then given by:

$$f(V > v \mid u) = \hat{\lambda} \times \mathrm{GPD}\left(\hat{\sigma}, \hat{\xi}\right) = \hat{\lambda} \times \left[1 + \hat{\xi}\left(\frac{v - u}{\hat{\sigma}}\right)\right]^{-1/\hat{\xi}} \quad (6)$$

where V represents the volume of the blocks (in m^3), $\hat{\lambda}$ is the temporal occurrence frequency of rockfall per unit of area (events/yr/hm^2), and u, $\hat{\sigma}$, $\hat{\xi}$ the location, scale and shape of the GPD distribution, respectively. The circumflex denotes statistical estimates obtained from the data using a maximum likelihood procedure.

3.3. Trajectory and maximum runout of falling blocks

Due to the scattering of the rockfall phenomenon, the propagation component must also be taken into account in rockfall hazard assessments (Crosta and Agliardi, 2003).

The proportion of risk analysis involving the interaction between rockfalls and elements at risk (i.e. impact probability and vulnerability) was supported by high-resolution 3D numerical modelling performed using the Rockyfor3D (v5.0) code (Dorren, 2012). On the basis of a digital elevation model, this probabilistic process-based rockfall trajectory model combines physically based deterministic algorithms with stochastic approaches to simulate rockfall in three dimensions. The model calculates sequences of classical, uniformly accelerated parabolic freefall through the air and rebounds on the slope surface and trees (for details see Dorren et al., 2005). During each rebound, the model allows the block to deviate from its direction before rebounding. If an impact against a tree takes place, part of the rock energy is dissipated as a function of the stem diameter of the corresponding tree and the relative position between the rock and tree center. LULC patchiness is explicitly integrated into Rockyfor3D through its spatial modelling features. The parameters used to characterise the interactions between the block and the soil – soil mechanical properties (i.e. restitution coefficients) and soil roughness – are implicitly related to LULC patterns. As outputs, the model provides, for example, information on rock propagation for any location in the study site such as the number, in the simulation sample, of passing rocks through a given surface or the mean of the maximum kinetic energy values of all simulated blocks in a given location.

In the transit area, Rockyfor3D uses a normal and a tangential coefficient of restitution to calculate rock rebound on the slope surface (Volkwein et al., 2011). The normal coefficient of restitution (r_n) defines the change in normal velocity during impact. In Rockyfor3D, r_n values are associated with slope materials depending on mechanical properties, i.e. the capacity of slope materials to dissipate energy. The tangential coefficient of restitution (r_t) defines the reduction in tangential velocity during impact. Both coefficients depend on (i) the rock shape and radius and (ii) the depth of the impact crater during a rebound (Dorren et al., 2005). Given that the composition and size of the material covering the slope surface and normal restitution coefficients are closely related to land use, they were translated into several LULC classes (Table 1; Table 2). The oldest forest allotments present in the upper part of the slopes, at the contact with the cliff, were mainly located on steep scree slopes. These forests have been assigned high surface roughness values (Rg10: 0.25 m; Rg20: 0.15 m; Rg70: 0.05 m). In contrast, limited roughness (Rg10: $\leq$ 0.05 m; Rg20: 0.0 m; Rg70: 0.0 m) was associated with cultivated land (i.e. grassland, farmland allotments) and urbanised areas. Finally, the protective walls were removed from the DEM and gaps were corrected using a spatial interpolation method.

3.4. Reach probability, mean damage and elements at risk

Quantitative risk assessment was performed for the four land-use and land-cover maps introduced above. This study does not account for rockfalls with volumes that exceed 20 m^3 so as to (i) preserve the efficiency of data storage and processing as well as to (ii) remain within the Rockyfor3D model validity range. Rockfall cell sources defined through the slope angle frequency distribution approach were mapped on the DEM and 10 000 rockfalls with volumes randomly extracted between 1 and 20 m^3 were simulated from each source cell. For each landscape pattern, the elements at risk considered in the analysis include the buildings currently existing in the Crolles urban map (Fig. 1C). In Rockyfor3D the latter are characterised as obstacles with infinite height and resistance. As a consequence, in case of any impact with an element at risk, each block is stopped. The original source code of Rockyfor3D was modified to enable the storage, for each simulation, of (i) the building reached, (ii) starting cell IDs, (iii) the volume of the block and (iv) its kinetic energy (in kJ). The results are recorded in a database used subsequently to compute the probability of an impact on the elements at risk z as:

$$p_z(V_{CL}) = \frac{Sim_z(V_{CL})}{Sim_{Tot}(V_{CL})} \quad (7)$$

where $p_z(V_{CL})$ is the reach probability on element at risk z for blocks belonging to the volume class V_{CL}. $Sim_z(V_{CL})$ is the total number of blocks simulated in the volume class V_{CL} that reach the element at risk z and $Sim_{TOT}(V_{CL})$ is the total number of blocks simulated in the volume class V_{CL}.

Impact energies recorded over the simulations which impact an element at risk were expressed as a damaging value on a structure. Considering that all the houses in Crolles were constructed using similar materials (e.g. masonry or reinforced concrete framing), damage values were obtained from the physical vulnerability curve of Agliardi et al. (2009), which derives the energy of impact as a potential degree of loss evolving between 0 (no structural damage) and 1 (total collapse). This curve results from the back-analysis of the 2004 rockfall event in Fiumelatte (Italy). It combines observed damage on structures and computed impact energies (through the HY-STONE code). Since an element at risk can be reached by a large number of simulations in a given volume class V_{CL}, its damage value is set by the mean of the distribution as following:

$$\overline{D_z}(V_{CL}) = \frac{1}{k} \sum_{k \in V_{CL}}^{n} 1 - \frac{1.358}{1 + e^{\frac{E_k - 129000}{120300}}} \quad (8)$$

where $\overline{D_z}\,(V_{CL})$ is the mean damage on element at risk z for blocks belonging to the volume class V_{CL}, and E_k is the impacted energy (in kJ) for the block belonging to the V_{CL} class.

Contrary to vehicles, trains and humans, buildings are static and consequently exposure factor $q(z_w) = 1$. Finally, the values z_w are defined as the floor area (m^2) approximated from the current cadastral map. The risk is thus expressed as the mean surface destroyed each year (m^2/yr).

4. Results

4.1. Rockfall frequency and release areas

The fitted generalised Pareto model is characterised by maximum likelihood estimators $\hat{\sigma}$ and $\hat{\xi}$ equal to 0.94 and 0.355, respectively (Fig. 4). The related uncertainty is obtained by propagating the maximum likelihood estimation asymptotic covariance matrix of the estimates using a delta-like approach. Based on the relative freshness of the blocks (limited patina, absence of blunt or rounded-off edges, lichens or vegetation on the surface) and the presence of visible scars on tree stems, we estimated that the reference period for the computation of rock frequency should not reasonably exceed one century. Based on this estimated timeframe, we inventoried 17 blocks greater than 1 m^3 potentially released from a 11.5-hm^2 cliff section located above the representative transect chosen for field analysis. As a consequence, the rockfall frequency $\hat{\lambda}$ was estimated at 0.015 events/yr/hm^2. According to the Histofit routine, the threshold slope angle for source areas was set at 49° and 20 331 cells were identified as potential rockfall release areas. These sources were evaluated to correspond to a total surface of 127.85 hm^2, and consequently the frequency of rockfalls greater than 1 m^3 and 20 m^3 were estimated at 1.89 and 0.005 events/yr, respectively. Last, since a limited distribution (up to 20 m^3) was considered, the frequencies per volume class $f(V_{CL})$ were normalised by $\int_{20}^{\infty} \mathrm{GPD}(\hat{\sigma}, \hat{\xi})$ to obtain a probability density function with a total probability of one.

4.2. Probability and energy of rockfall impacts

The database obtained from the rockfall simulations was used to estimate probabilities and energies of rockfall impacts. These were interpreted at the level of each individual house as well as at the municipality scale (i.e. regardless of the single elements at risk), for all the volume classes or in specific volume ranges.

In the binary pattern, the landscape is characterised by a continuous forest strip at the base of the cliff and the presence of vineyards below 450 m a.s.l. (Fig. 2A). At the municipality scale, and regardless of the volume class, 1 115 111 impacts, homogeneously distributed at the scale of the urban front, were recorded on 342 buildings (Fig. 5A). A total of 96% of the impacted buildings had an individual reach probability (p_z) below 0.01% while p_z never exceed 0.05% (Table 3). The impacts were not restricted to the upper portion of the urban front, but blocks passing in the intervals between houses reached the sixth row of buildings in, for example, the Coteau neighbourhood (Fig. 5A). In addition, the kinematic energies exceeded 1000 kJ for 85% of the impacts and are typically associated with volumes greater than 10m^3.

In the mosaic A pattern, despite the widening of the forest strip on the upper part of the slope (from 36 to 51% of the total surface) (Fig. 2B), the number of blocks that reached the urban front was multiplied by almost 10. In contrast, the 11 320 596 impacts were distributed over a more limited number of buildings (263) (Fig. 5B). The individual reach probability p_z exceeded 0.05 for 19 (7%) elements at risk (Table 3). Overall, the impact energies were lower and did not exceed 1000 kJ for 61% of the impacts.

The mosaic B pattern differed from mosaic A in its limited afforestation (+6%) (Fig. 2C), but the density of the forest stand in Rockyfor3D increased from 1000 to 1500 trees/ha (Table 2). This change in the forest stand structure induced a sharp decrease in the total number of impacts (1 267 674). The number of impacted buildings remained stable (260) (Fig. 5C), yet p_z exceeded 0.05% for three buildings that concentrated 35% of the total number of simulated impacts. Energies greater than 1000 kJ accounted for 66% of the impacts.

Finally, in the last pattern implemented in rockfor3D - representative of the current landscape at Crolles (Fig. 2D) – 1 645 834 impacts were recorded on 177 buildings (Fig. 5D). The impacts were restricted to the first two rows of exposed buildings. In total, 92% of the impacted elements at risk had a reach probability p_z less than 0.01%, but two buildings located in the Coteau neighbourhood were characterised by a p_z value greater than 0.05%. Interestingly, they accounted for 10 and 42% of the total number of recorded impacts, respectively. The increase of forest coverage (+11% wrt mosaic B pattern) induced a substantial dissipation of block energies, with only 41% of impacts exceeding 1000 kJ at the level of the urban front.

Maximum energies of 78 400 kJ (block volume, 20 m^3), 70 700 kJ (block volume, 19 m^3), 75 300 kJ (block volume, 20 m^3) and 66 400 kJ (block volume, 18 m^3) were recorded for the binary, mosaic A, mosaic B and densely forested patterns, respectively.

345

346 4.3. Vulnerability and risk analysis results

347

348 The energies of rockfall impacts at the level of each element at risk were converted to an expected damage level
349 based on the empirical vulnerability function developed by Agliardi et al. (2009). In the binary pattern, the means
350 of the damage distribution of volume classes above 5 m^3 were always higher than 0.9. For smaller volumes,
351 distributions were more scattered (Fig. 6), but the mean damage values remained above 0.8 regardless of the
352 volume class. In the mosaic A pattern, the energy of the blocks that reached the urban front was considerably
353 reduced irrespective of the volume. Comparing the binary and mosaic A patterns, the mean damage induced by
354 blocks whose volume was in the classes 1-2, 5-6, 10-11 m^3, for example, decreased from 0.8 to 0.3, 0.9 to 0.5 and
355 0.9 to 0.75, respectively. In mosaic B, the mean damage value (0.75) for 1- to 2-m^3 blocks was comparable to the
356 binary pattern and varied between 0.8 and 0.9 for volume classes above 2 m^3 (Fig. 6). Finally, in the densely
357 forested pattern, despite the lower number of blocks that reached the urban front, the mean damage was greater
358 than in mosaic A for volume classes up to 7 m^3. Conversely, the energies of the largest class volumes were lower in
359 the densely forested pattern, the mean damage decreasing from, for example, 0.75 to 0.6 and 0.9 to 0.8 for the
360 volume classes 10-11 m^3 and 19-20 m^3, respectively.
361 Following Eq4 and Eq5 - which combine the rockfall frequency, the individual reach probability and the mean
362 degree of loss of each element at risk, for each volume class (Fig. 3) - we computed the risk to buildings in terms
363 of mean annual destroyed surface per year (m^2/yr). Following this approach, the mean total risk R_w decreased from
364 0.2 to 0.1 m^2/year between the binary and the densely forested patterns. Despite the progressive afforestation of
365 the slope (from 36 to 68%), it should be stressed that the risk did not decrease linearly. Mosaic patterns A and B
366 were characterised by destroyed surfaces ten times greater than (1.1 m^2/yr) and similar to the binary pattern (0.2
367 m^2/yr), respectively. In detail, the individual risk was less than 0.001 m^2/yr for the vast majority of the impacted
368 buildings for each pattern (Fig. 5). If we consider a typical structure of 150 m^2, this value corresponds to the
369 complete destruction of the building every 150 000 years. On the other hand, it exceeds 0.01 m^2/yr for 5, 21, 4 and
370 1 buildings for the binary, mosaic A, mosaic B and densely forested patterns, respectively, but the location of these
371 most impacted elements changes depending on landscape patterns (Fig. 5).
372 Figure 7 shows the risk for each pattern depending on the 19 volume classes. Each distribution is compared with
373 the expected risk value when the degree of loss is set at a value of 1. With the exception of volume classes less
374 than 2 m^3, both distributions collapsed for binary and mosaic B patterns. Conversely, for the mosaic A and densely
375 forested patterns, the discrepancies between the two distributions induced a difference of 38 and 35% in the

rockfall risk, respectively. These differences illustrate the influence of energy on the risk, namely the ability of masonry walls to resist "low" energy impacts.

In addition, for all the patterns, the distributions of risk with maximum and mean degrees of loss presented a single peak. This peak was observed for similar volume classes (2-3 m^3) for the binary and mosaic B patterns, whereas they occurred for volume classes 8-9 and 10-11 m^3 in the case of binary and densely forested patterns, respectively. The shift of these peaks from 1-2 m^3 to higher values evidences the non-linear relationship between reach probabilities and volumes directly related to the influence of landscape structures.

5. Discussion

5.1. Impacts of landscape organisation on rockfall risk

In this study, we developed a quantitative analysis of rockfall risk in the municipality of Crolles (French Alps). To integrate a wide spectrum of probability of occurrence, propagation, intensity, impact probability and resulting damage to buildings, the complete distribution of block volumes in the range 1-20 m^3 was implemented in our rockfall risk calculation. Applied to four LULC patterns representative of the landscape observed on south-facing calcareous slopes in several alpine valleys, this provides a better understanding of the interactions between the landscape structure and the rockfall risk. The results were presented at the level of each building and at the municipality scale, in order to map the most risk-prone areas and to identify the impacts of LULC changes on the overall risk, respectively. Unsurprisingly, these results demonstrate that the risk was reduced by a factor of 2 as a result of the intense afforestation process observed between the binary and densely forested patterns (+32%). This reduction is attributed to forest-block interactions that significantly reduce both the reach probability and the energy of rockfalls (Dupire et al., 2016a; Dupire et al., 2016b; Toe et al., 2018). In the densely forested pattern, our analysis demonstrates that the high and dense forest cover has a significant influence on rockfall risk associated with lower volumes, but its protective function is limited for rock volumes greater than 10 m^3. These results are consistent with the findings of Moos et al. (2017) at two sites in the Swiss Alps, demonstrating that risk is strongly reduced (between 20 and 50%) in forest areas for volumes less than 5 m^3 but can remain considerable for greater volumes when forested slopes are sufficiently long. On a spatial plan, the comparison of risk maps shows (i) changing distributions of exposed buildings for each pattern and (ii) a risk limited to the first exposed buildings in the densely forested pattern. In greater detail, the existence of critical risk-prone areas in the densely forested pattern seems to result from specific terrain conditions and LULC patterns, as observed in the Coteau

neighbourhood where the most impacted building (42% of reach probability, 27% of the total risk) is overhung by a grassland plot located downslope from a preferential corridor (Fig. 8). To a certain extent, these results validate the observations on virtual slopes that have shown the importance of forest fragmentation on the reduction of rockfall intensity and, more specifically, demonstrated that the kinetic energies of blocks are significantly higher in forest stands with a clustered tree structure and in forests with gaps or aisles compared to random tree distribution (Dupire et al., 2016b; Toe et al., 2018).

More interestingly, despite a wider and denser forest strip, the risk does not decrease gradually and is, for example, ten times greater in mosaic A than in the binary pattern. We hypothesise that this paradoxical evolution is mainly driven by the evolution of soil mechanical properties implemented in Rockyfor3D, with vineyards (Rg10=0.10, Rg20=0.05, Rg70=0, Rn=0.23) more likely to stop or decelerate blocks and to reduce their energy than grassland characterised by an absence of roughness and larger normal restitution coefficients (R_n=0.28; Table 1). This hypothesis is further supported by the propagation maps for the binary pattern showing the large proportion of rockfalls stopped in the vineyard allotments (above 300 m a.s.l.). The protection function of the forest should not be underestimated in the mosaic A pattern since we demonstrated its impacts on propagation for lower volume classes (Fig. 7). Yet, the expansion of the forest strip remains insufficient to compensate for the loss of roughness stemming from grassland expansion.

Finally, for mosaic B, R_w is (i) comparable to the binary pattern, but the risk is less diffuse on the urban front and clustered in a limited number of risk-prone areas and (ii) considerably lower than mosaic A despite limited differences in LULC patterns. These discrepancies could be explained by the expansion of wood formation (forest and untilled land) on grassland and concomitant increasing roughness in the most concave portion of the slope (Lopez-Saez et al., 2016) and to a lesser extent the increase in forest density.

All in all, these results suggest a key role played by the landscape structure and the associated roughness on rockfall risk, especially with respect to low-volume/high-frequency classes, and clearly evidence that the risk reduction associated with continuous afforestation can be significantly counterbalanced by landscape reorganisation below the forest front. Similar effects of LULC changes have been reported for snow avalanche risk (García-Hernández et al., 2017). By contrast, the scarce existing literature devoted to the non-stationarity of rockfall processes mainly focuses on recent high-altitude changes under climate warming (e.g. Ravanel and Deline, 2011). By focusing on LULC changes and explicitly quantifying the risk at a lower-altitude location where the population is rapidly increasing, our results complement the current knowledge and broaden the perspective, opening the door to the assessment of the complete response of a complex system to substantial simultaneous physical, environmental and societal changes.

438

439 5.2. Novelty and limitations of the quantitative risk analysis approach undertaken at Crolles

440

441 Rockfall risk studies are usually based on the retro-analysis of rockfall events (Agliardi et al., 2009) to implement a
442 restricted number of rockfall volumes released from critical areas. Here, in order to propose a more holistic risk
443 analysis, we considered all the release areas that potentially threaten the village studied as well as the complete
444 distribution of rockfall volumes ranging from 1 to 20 m^3. In addition, a power-law approach is commonly used to
445 characterise rockfall frequencies (Dussauge-Peisser et al., 2002; Lopez-Saez et al., 2016). By contrast, we used a
446 volume-cumulative frequency relationship fitted by an asymptotic model of the generalised Pareto distribution.
447 This approach has been demonstrated to be more suitable to quantifying the stochastic behaviour of numerous
448 occurrences of any process in a generic way (Coles, 2001), especially in the context of natural hazard assessment
449 (e.g. Evin et al., 2018; Favier et al., 2016). For each building, risk maps resulting from our analyses characterise a
450 probability of physical losses due to rockfalls. Furthermore, the implementation of the complete spectra of rockfall
451 volumes in our QRA procedure provides a robust understanding of the risk distribution associated with each volume
452 class. This approach is of major interest for stakeholders in charge of risk management because it allows for
453 prioritising and designing mitigation measures (Corominas et al., 2013, 2005). In addition, and in contrast to the
454 current practices in which risk is usually expressed as damage in monetary values (Agliardi et al., 2009; Moos et al.,
455 2017), we deliberately quantified the risk as a physical loss expressed in m^2/yr. The choice of this metric -
456 independent of the spatial and temporal variability of the property prices - also guarantees the reproducibility of
457 the procedure and facilitates site-by-site comparison. Finally, the implementation of LULC patterns in this analysis
458 made it possible to document the impacts of landscape evolution on rockfall risk and ensures its replicability to a
459 wide range of calcareous south-facing slopes in the Alps. The use of realistic landscape scenario changes allows
460 rockfall risk analyses to be performed in a non-stationary context, which are urgently needed given the quick and
461 consequential changes now affecting the environment in which mountain hazards arise (Beniston et al., 2018;
462 Giacona et al., 2018). It could also be used in further work for a precise monetisation of ecosystem services, most
463 particularly those related to the protective function of different landscape patterns.
464 Despite its high interest for stakeholders, one must keep in mind that our methodology is based on several
465 assumptions inherent to quantitative risk analyses (Straub and Schubert, 2008) and related to (i) the magnitude and
466 frequency of rockfall, (ii) rockfall propagation and (iii) the scarcity of vulnerability relations in the existing
467 literature. With regard to the frequency distribution of rockfall volumes, the lack of a statistically representative
468 catalogue of rockfall events has been overcome at Crolles through detailed field observations along a

representative transect. Despite exhaustive field investigations, inaccuracies remain in this rockfall catalogue due to (i) highly probable rock removal in the lower part of the slope and (ii) potential biases on the volume and frequency estimations related to potential fragmentation during rockfall propagation (Corominas and Mavrouli, 2013). Regarding rockfall propagation (Bourrier et al., 2009), technical restrictions concern the ability of the Rockyfor3D simulation model to properly simulate rockfall trajectories for large volumes. Furthermore, soil mechanical properties attributed to each of the allotments remain difficult to estimate and the results reported herein, in agreement with Corona et al. (2017), demonstrate that slight variations in roughness parameters in the rockfall simulation model induce significant changes in energy loss and runout distance. Finally, damage assessment is based on the vulnerability function specifically developed by Agliardi et al. (2009) for the Fiumelatte (Italy) site. The choice of this function was driven by (i) comparable slope lengths (>500 m) and rockfall volume classes at Crolles and Fiumelatte, (ii) the lack of damaging events at Crolles that would have enabled a site-specific retro-analysis and (iii) the scarcity of vulnerability curves for structural elements in the existing literature. For example, the approach developed by Mavrouli and Corominas (2010), which accounts for the impact location of the rock and requires detailed information on the structure, was not applicable at our study site scale. Yet, the results should be considered cautiously because (i) the vulnerability curve of Agliardi et al. (2009) was calibrated on a limited number of documented events and (ii) it is impossible to precisely evaluate the relevance of this transposition. In view of these different limitations, the risk values obtained in this study can be considered indicative (Corominas et al., 2013), but further work is certainly required to evaluate the weight of the different assumptions made on the final risk estimates. Specifically, a systematic quantification of uncertainties associated with each of the risk components would greatly improve the reliability of the results (Straub and Schubert, 2008; Wang et al., 2014).

Conclusion and outlooks

In this study, we developed a quantitative analysis of rockfall risk in Crolles that integrates (i) four different land-use and land-cover patterns representative of observed landscapes on calcareous slopes in different periurban regions in the Alps, (ii) the complete distributions of rock volumes in the 1-to 20-m^3 range and (iii) all potential release areas in order to assess the risk for a wide spectrum of patterns at the level of the current urban front. As expected, the risk decreased significantly as the afforestation of the slope increased. Yet, we demonstrated that the risk decrease is not gradual and that the positive effect of increasing forest cover can be strongly counterbalanced by landscape reorganisation (e.g. vineyard replaced with grassland) in the transition area located

between the forest and the urban front. In addition, the approach developed here, at the municipality scale, not only precisely maps the elements highly subjected to risk, but also evidences significant changes in the risk patterns for different landscapes. These results, transposable to a wide range of calcareous south-facing slopes in the Alps, can quantify the protection value of the landscape. They also demonstrate the added value of a dynamic approach accounting for LULC changes for risk assessment. In the future, a similar procedure that would integrate socio-economic evolution such as urban sprawl is encouraged and would provide a complete and more reliable risk analysis. Finally, an additional key finding of the present study is that the evolution in rockfall risk is mainly driven by lower-volume classes. This result carried even greater interest in that for these volume classes both frequency and propagation could be potentially greatly affected by ongoing environmental changes in alpine regions (land abandonment) as well as global warming. Although the limitations mentioned in the Discussion should be kept in mind, they clearly demonstrate the practicability of the QRA at a municipality scale and its major value in terms of risk zoning in a context of significant and rapid socio-environmental change.

Acknowledgments

This research was funded by a Ph.D. grant from Rhône-Alpes Region – ARC Environnement 3, the C2ROP (Chutes de blocs, Risques Rocheux, Ouvrages de Protection) national research project and the Irstea ZORRINO (Zonage réglementaire du risque en montagne par optimisation des pertes) project. This work is also supported by the French National Research Agency in the framework of the Investissements d'Avenir program (ANR-15-IDEX-02). It was conducted within the Risk@Univ. Grenoble Alpes cross-disciplinary program. Irstea is member of Labex Osug@2020.

533
534
535
536

537 **References**

538

539 Agliardi, F., Crosta, G.B., Frattini, P., 2009. Integrating rockfall risk assessment and countermeasure design by 3D
540 modelling techniques. Nat. Hazards Earth Syst. Sci. 9, 1059–1073. https://doi.org/10.5194/nhess-9-1059-
541 2009

542 Assali, P., 2015. Modélisation géostructurale 3D de parois rocheuses par lasergrammétrie et photogrammétrie
543 terrestres en milieu ferroviaire. Bull. Eng. Geol. Environ. 74, 1255–1265. https://doi.org/10.1007/s10064-
544 014-0711-8

545 Badoux, A., Andres, N., Techel, F., Hegg, C., 2016. Natural hazard fatalities in Switzerland from 1946 to 2015. Nat.
546 Hazards Earth Syst. Sci. 16, 2747–2768. https://doi.org/10.5194/nhess-16-2747-2016

547 Beniston, M., Farinotti, D., Stoffel, M., Andreassen, L.M., Coppola, E., Eckert, N., Fantini, A., Giacona, F., Hauck,
548 C., Huss, M., Huwald, H., Lehning, M., López-Moreno, J.-I., Magnusson, J., Marty, C., Morán-Tejéda, E.,
549 Morin, S., Naaim, M., Provenzale, A., Rabatel, A., Six, D., Stötter, J., Strasser, U., Terzago, S., Vincent,
550 C., 2018. The European mountain cryosphere: a review of its current state, trends, and future challenges.
551 The Cryosphere 12, 759–794. https://doi.org/10.5194/tc-12-759-2018

552 Bourrier, F., Baroth, J., Lambert, S., 2016. Accounting for the variability of rock detachment conditions in
553 designing rockfall protection structures. Nat. Hazards 81, 365–385. https://doi.org/10.1007/s11069-015-
554 2084-0

555 Bourrier, F., Dorren, L., Nicot, F., Berger, F., Darve, F., 2009. Toward objective rockfall trajectory simulation
556 using a stochastic impact model. Geomorphology 110, 68–79.
557 https://doi.org/10.1016/j.geomorph.2009.03.017

558 Brabb, 1984. Innovative Approaches for Landslide Hazard Evaluation. Presented at the IV International Symposium
559 on Landslides, Toronto, pp. 307–323.

560 Budetta, P., 2004. Assessment of rockfall risk along roads. Nat. Hazards Earth Syst. Sci. 4, 71–81.
561 https://doi.org/10.5194/nhess-4-71-2004

562 Budetta, P., Nappi, M., 2013. Comparison between qualitative rockfall risk rating systems for a road affected by
563 high traffic intensity. Nat. Hazards Earth Syst. Sci. 13, 1643–1653. https://doi.org/10.5194/nhess-13-1643-
564 2013

Coles, S., 2001. An Introduction to Statistical Modeling of Extreme Values, Springer Series in Statistics. Springer London, London. https://doi.org/10.1007/978-1-4471-3675-0

Corominas, J., Copons, R., Moya, J., Vilaplana, J.M., Altimir, J., Amigó, J., 2005. Quantitative assessment of the residual risk in a rockfall protected area. Landslides 2, 343–357. https://doi.org/10.1007/s10346-005-0022-z

Corominas, J., Mavrouli, O., 2013. Rockfall Quantitative Risk Assessment, in: Lambert, S., Nicot, F. (Eds.), Rockfall Engineering. John Wiley & Sons, Inc., Hoboken, NJ, USA, pp. 255–301. https://doi.org/10.1002/9781118601532.ch8

Corominas, J., van Westen, C., Frattini, P., Cascini, L., Malet, J.-P., Fotopoulou, S., Catani, F., Van Den Eeckhaut, M., Mavrouli, O., Agliardi, F., Pitilakis, K., Winter, M.G., Pastor, M., Ferlisi, S., Tofani, V., Hervás, J., Smith, J.T., 2013. Recommendations for the quantitative analysis of landslide risk. Bull. Eng. Geol. Environ. https://doi.org/10.1007/s10064-013-0538-8

Corona, C., Lopez-Saez, J., Favillier, A., Mainieri, R., Eckert, N., Trappmann, D., Stoffel, M., Bourrier, F., Berger, F., 2017. Modeling rockfall frequency and bounce height from three-dimensional simulation process models and growth disturbances in submontane broadleaved trees. Geomorphology 281, 66–77. https://doi.org/10.1016/j.geomorph.2016.12.019

Crosta, G.B., Agliardi, F., 2003. A methodology for physically based rockfall hazard assessment. Nat. Hazards Earth Syst. Sci. 3, 407–422. https://doi.org/10.5194/nhess-3-407-2003

D'Amato, J., Hantz, D., Guerin, A., Jaboyedoff, M., Baillet, L., Mariscal, A., 2016. Influence of meteorological factors on rockfall occurrence in a middle mountain limestone cliff. Nat. Hazards Earth Syst. Sci. 16, 719–735. https://doi.org/10.5194/nhess-16-719-2016

De Biagi, V., Napoli, M.L., Barbero, M., Peila, D., 2017. Estimation of the return period of rockfall blocks according to their size. Nat. Hazards Earth Syst. Sci. 17, 103–113. https://doi.org/10.5194/nhess-17-103-2017

Dorren, L.K.., 2012. Rockyfor3D (v5.1) revealed – Transparent description of the complete 3D rockfall model. 32.

Dorren, L.K.A., Berger, F., le Hir, C., Mermin, E., Tardif, P., 2005. Mechanisms, effects and management implications of rockfall in forests. For. Ecol. Manag. 215, 183–195. https://doi.org/10.1016/j.foreco.2005.05.012

Dupire, S., Bourrier, F., Monnet, J.-M., Bigot, S., Borgniet, L., Berger, F., Curt, T., 2016a. The protective effect of forests against rockfalls across the French Alps: Influence of forest diversity. For. Ecol. Manag. 382, 269–279. https://doi.org/10.1016/j.foreco.2016.10.020

595 Dupire, S., Bourrier, F., Monnet, J.-M., Bigot, S., Borgniet, L., Berger, F., Curt, T., 2016b. Novel quantitative
596 indicators to characterize the protective effect of mountain forests against rockfall. Ecol. Indic. 67, 98–
597 107. https://doi.org/10.1016/j.ecolind.2016.02.023
598 Dussauge-Peisser, C., Helmstetter, A., Grasso, J.-R., Hantz, D., Desvarreux, P., Jeannin, M., Giraud, A., 2002.
599 Probabilistic approach to rock fall hazard assessment: potential of historical data analysis. Nat. Hazards
600 Earth Syst. Sci. 2, 15–26. https://doi.org/10.5194/nhess-2-15-2002
601 Eckert, N., Keylock, C.J., Bertrand, D., Parent, E., Faug, T., Favier, P., Naaim, M., 2012. Quantitative risk and
602 optimal design approaches in the snow avalanche field: Review and extensions. Cold Reg. Sci. Technol. 79–
603 80, 1–19. https://doi.org/10.1016/j.coldregions.2012.03.003
604 Eckert, N., Naaim, M., Giacona, F., Favier, P., Lavigne, A., Richard, D., Bourrier, F., Parent, E., 2018. Repenser les
605 fondements du zonage règlementaire des risques en montagne « récurrents ». Houille Blanche 38–67.
606 https://doi.org/10.1051/lhb/2018019
607 Einhorn, B., Eckert, N., Chaix, C., Ravanel, L., Deline, P., Gardent, M., Boudières, V., Richard, D., Vengeon, J.-M.,
608 Giraud, G., Schoeneich, P., 2015. Climate change and natural hazards in the Alps: Observed and potential
609 impacts on physical and socio-economic systems. Rev. Géographie Alp. https://doi.org/10.4000/rga.2878
610 Erismann, T.H., Abele, G., 2001. Dynamics of Rockslides and Rockfalls. Springer Berlin Heidelberg, Berlin,
611 Heidelberg. https://doi.org/10.1007/978-3-662-04639-5
612 Evin, G., Curt, T., Eckert, N., 2018. Has fire policy decreased the return period of the largest wildfire events in
613 France? A Bayesian assessment based on extreme value theory. Nat. Hazards Earth Syst. Sci. 18, 2641–
614 2651. https://doi.org/10.5194/nhess-18-2641-2018
615 Favier, P., Eckert, N., Faug, T., Bertrand, D., Naaim, M., 2016. Avalanche risk evaluation and protective dam
616 optimal design using extreme value statistics. J. Glaciol. 62, 725–749.
617 https://doi.org/10.1017/jog.2016.64
618 Fell, Ho, Lacasse, Leroi, 2005. A framework for landslide risk assessment and management. Landslide Risk Manag.
619 Fell, R., Corominas, J., Bonnard, C., Cascini, L., Leroi, E., Savage, W.Z., 2008. Guidelines for landslide
620 susceptibility, hazard and risk zoning for land use planning. Eng. Geol. 102, 85–98.
621 https://doi.org/10.1016/j.enggeo.2008.03.022
622 Ferrari, F., Giacomini, A., Thoeni, K., 2016. Qualitative Rockfall Hazard Assessment: A Comprehensive Review of
623 Current Practices. Rock Mech. Rock Eng. 49, 2865–2922. https://doi.org/10.1007/s00603-016-0918-z

Field, C.B., Intergovernmental Panel on Climate Change (Eds.), 2012. Managing the risks of extreme events and disasters to advance climate change adaption: special report of the Intergovernmental Panel on Climate Change. Cambridge University Press, New York, NY.

García-Hernández, C., Ruiz-Fernández, J., Sánchez-Posada, C., Pereira, S., Oliva, M., Vieira, G., 2017. Reforestation and land use change as drivers for a decrease of avalanche damage in mid-latitude mountains (NW Spain). Glob. Planet. Change 153, 35–50. https://doi.org/10.1016/j.gloplacha.2017.05.001

Giacona, F., Eckert, N., Mainieri, R., Martin, B., Corona, C., Lopez-Saez, J., Monnet, J.-M., Naaim, M., Stoffel, M., 2018. Avalanche activity and socio-environmental changes leave strong footprints in forested landscapes: a case study in the Vosges medium-high mountain range. Ann. Glaciol. 1–23. https://doi.org/10.1017/aog.2018.26

Grandvoinnet, P., 2011. Les emprises militaires dans l'urbanisme grenoblois du XXe siècle : des opportunités foncières au patrimoine paysager. Situ. https://doi.org/10.4000/insitu.217

Hackl, J., Lam, J.C., Heitzler, M., Adey, B.T., Hurni, L., 2018. Estimating the risk related to networks: a methodology and an application on a road network. Nat. Hazards Earth Syst. Sci. Discuss. 1–41. https://doi.org/10.5194/nhess-2017-446

Hantz, D., 2013. Gestion de l'incertitude et de l'ignorance, dans l'évaluation de la probabilité de déclenchement des éboulements rocheux.

Haque, U., Blum, P., da Silva, P.F., Andersen, P., Pilz, J., Chalov, S.R., Malet, J.-P., Auflič, M.J., Andres, N., Poyiadji, E., Lamas, P.C., Zhang, W., Peshevski, I., Pétursson, H.G., Kurt, T., Dobrev, N., García-Davalillo, J.C., Halkia, M., Ferri, S., Gaprindashvili, G., Engström, J., Keellings, D., 2016. Fatal landslides in Europe. Landslides 13, 1545–1554. https://doi.org/10.1007/s10346-016-0689-3

Kamada, M., Nakagoshi, N., 1997. Influence of cultural factors on landscapes of mountainous farm villages in western Japan. Landsc. Urban Plan. 37, 85–90. https://doi.org/10.1016/S0169-2046(96)00372-6

Lari, S., Frattini, P., Crosta, G.B., 2014. A probabilistic approach for landslide hazard analysis. Eng. Geol. 182, 3–14. https://doi.org/10.1016/j.enggeo.2014.07.015

Lopez-Saez, J., Corona, C., Eckert, N., Stoffel, M., Bourrier, F., Berger, F., 2016. Impacts of land-use and land-cover changes on rockfall propagation: Insights from the Grenoble conurbation. Sci. Total Environ. 547, 345–355. https://doi.org/10.1016/j.scitotenv.2015.12.148

Loye, A., Jaboyedoff, M., Pedrazzini, A., 2009. Identification of potential rockfall source areas at a regional scale using a DEM-based geomorphometric analysis. Nat. Hazards Earth Syst. Sci. 9, 1643–1653. https://doi.org/10.5194/nhess-9-1643-2009

Mavrouli, O., Corominas, J., 2010. Rockfall vulnerability assessment for reinforced concrete buildings. Nat. Hazards Earth Syst. Sci. 10, 2055–2066. https://doi.org/10.5194/nhess-10-2055-2010

Michoud, C., Derron, M.-H., Horton, P., Jaboyedoff, M., Baillifard, F.-J., Loye, A., Nicolet, P., Pedrazzini, A., Queyrel, A., 2012. Rockfall hazard and risk assessments along roads at a regional scale: example in Swiss Alps. Nat. Hazards Earth Syst. Sci. 12, 615–629. https://doi.org/10.5194/nhess-12-615-2012

Moos, C., Fehlmann, M., Trappmann, D., Stoffel, M., Dorren, L., 2017. Integrating the mitigating effect of forests into quantitative rockfall risk analysis – Two case studies in Switzerland. Int. J. Disaster Risk Reduct. https://doi.org/10.1016/j.ijdrr.2017.09.036

Noetzli, J., 2003. Mountain permafrost and recent Alpine rock-fall events: a GIS-based approach to determine critical factors. Balkema Publishers. https://doi.org/10.5167/uzh-33321

Pickands, J., 1975. Statistical Inference Using Extreme Order Statistics. Ann. Stat. 3, 119–131. https://doi.org/10.1214/aos/1176343003

Ravanel, L., Deline, P., 2011. Climate influence on rockfalls in high-Alpine steep rockwalls: The north side of the Aiguilles de Chamonix (Mont Blanc massif) since the end of the 'Little Ice Age.' The Holocene 21, 357–365. https://doi.org/10.1177/0959683610374887

Romero-Calcerrada, R., Perry, G.L.W., 2004. The role of land abandonment in landscape dynamics in the SPA 'Encinares del rı▫o Alberche y Cofio, Central Spain, 1984–1999. Landsc. Urban Plan. 66, 217–232. https://doi.org/10.1016/S0169-2046(03)00112-9

Stevenson, I., 1980. The diffusion of disaster: The phylloxera outbreak in the département of the Hérault, 1862–1880. J. Hist. Geogr. 6, 47–63. https://doi.org/10.1016/0305-7488(80)90043-2

Stoffel, M., Huggel, C., 2012. Effects of climate change on mass movements in mountain environments. Prog. Phys. Geogr. 36, 421–439. https://doi.org/10.1177/0309133312441010

Straub, D., Schubert, M., 2008. Modeling and managing uncertainties in rock-fall hazards. Georisk Assess. Manag. Risk Eng. Syst. Geohazards 2, 1–15. https://doi.org/10.1080/17499510701835696

Tasser, E., Tappeiner, U., 2002. Impact of land use changes on mountain vegetation. Appl. Veg. Sci. 5, 173–184. https://doi.org/10.1111/j.1654-109X.2002.tb00547.x

Toe, D., Bourrier, F., Dorren, L., Berger, F., 2018. A Novel DEM Approach to Simulate Block Propagation on Forested Slopes. Rock Mech. Rock Eng. 51, 811–825. https://doi.org/10.1007/s00603-017-1348-2

Varnes, D., 1978. Slope movement types and processes, in: Schuster, R.L., Krizek, R.J. (Eds.), In Special Report 176. -Landslides: Analysis and Control, Transp. Res. Board. National Research Council, Washington, D.C. pp. 11–33.

Varnes, D.J., 1984. Landslide hazard zonation: a review of principles and practice, Natural hazards. Unesco, Paris.

Veyret-Verner, G., 1937. L'agriculture du Grésivaudan. Rev. Géographie Alp. 25, 273–346. https://doi.org/10.3406/rga.1937.4076

Volkwein, A., Schellenberg, K., Labiouse, V., Agliardi, F., Berger, F., Bourrier, F., Dorren, L.K.A., Gerber, W., Jaboyedoff, M., 2011. Rockfall characterisation and structural protection – a review. Nat. Hazards Earth Syst. Sci. 11, 2617–2651. https://doi.org/10.5194/nhess-11-2617-2011

Walther, P., 1986. Land Abandonment in the Swiss Alps: A New Understanding of a Land-Use Problem. Mt. Res. Dev. 6, 305. https://doi.org/10.2307/3673371

Wang, X., Frattini, P., Crosta, G.B., Zhang, L., Agliardi, F., Lari, S., Yang, Z., 2014. Uncertainty assessment in quantitative rockfall risk assessment. Landslides 11, 711–722. https://doi.org/10.1007/s10346-013-0447-8

Fig. 1. (A-B) The pre-alpine conurbation of Crolles is located in the Isère valley, near the city of Grenoble, on the southeastern slopes of the Chartreuse Massif (French Alps); (C) General view of Crolles and the potential rockfall release areas. The urban plan is divided into four neighbourhoods, namely Le Fragnès, Magny, Ardillais and Le Coteau; (D-E) Historical photograph of Lumbin talus slope (close neighbour of Crolles) in 1911 (D) and a current photograph of the talus slope in 2017 (E).

Fig. 2. Land-use and land-cover (LULC) maps of the Crolles slopes for the binary pattern, the mosaic A pattern, the mosaic B pattern and the densely forested pattern.

Fig. 3. General scheme of the framework used to quantity the rockfall risk with regards to the volume class V_{CL}. The methodology is sumarised in five main steps: (1) estimating the rockfall frequency in class V_{CL} according to the adopted volume-cumulative frequency relationship, (2) rockfall propagation through the Rockyfor3D code, (3) calculating the reach probability p_z on each element at risk *z* related to volume class V_{CL}, (4) converting the related impact energies as a degree of loss to determine the mean damage for the element z and (5) assess the risk as the mean surface destroyed each year by integrating the raster surface. Total risk is obtained by an additional summation over the different volume classes.

Fig. 4. Volume-cumulative frequency relationship in events/yr/hm^2 (red line) obtained by an asymptotic model of the generalised Pareto distribution (GPD) family and related to rock volumes inventoried along a transect located in the Ardillais neighbourhood. The shaded area illustrates the model 95% confidence interval.

Fig. 5. Distribution of the rockfall risk (m^2/yr) at Crolles for the binary and the mosaic A patterns.

Fig. 5. (**Continued**) Distribution of the rockfall risk (m^2/yr) at Crolles for the mosaic B and densely forested patterns.

Fig. 6. Density function of the damage for each pattern and block volumes in the range of volumes 1-2 m^3, 2-3 m^3, 3-4 m^3, 4-5 m^3.

743 **Fig. 7.** Distribution of the rockfall risk in the 19 volume classes and for each landscape pattern. Each distribution is
744 compared with the risk distribution when the physical vulnerability is set at a value of 1 (total destruction of the
745 building as soon as it is hit, red line).
746
747 **Fig. 8.** (A) Estimation of the reach probabilities on buildings of Le Coteau from Rockyfor3D numerical modelling
748 results and for the densely forested pattern. These results are mapped on the aerial picture of the area (B) to
749 evidence specific terrain conditions (grassland plot located downslope of a preferential couloir).

LULC type		Rg70	Rg20	Rg10	R_n
Cliff		0	0	0.05	0.53
Scree		0.1	0.2	0.35	0.38
Vineyard		0	0.05	0.1	0.23
Crops		0	0	0.05	0.28
Grassland		0	0	0	0.28
Thalweg		0.25	0.5	0.7	0.38
Vegetated thalweg		0.25	0.5	0.7	0.28
Wasteland		0.05	0.1	0.1	0.28
Historical forest		0.05	0.15	0.25	0.33
Forest	Mosaic patterns A and B	0.05	0.1	0.2	0.33
	Densely forested pattern	0.05	0.15	0.25	0.33

Table 1. LULC and related soil characteristics implemented in Rockyfor3D. Rg70, Rg20 and Rg10 correspond to the slope surface roughness (obstacles for the falling block lying on the slope) for 70%, 20% and 10% of the surface, respectively. R_n value (normal coefficient of restitution) defines the change in normal velocity during impact and is associated with the different soil types (Dorren, 2012).

LULC type	Pattern	Nb.trees.ha	DBH mean	DBH std
Scree	All	400	5	2
Vegetated thalweg / wasteland	Binary	200	10	5
	Mosaic A, mosaic B and densely forested	400	10	5
Historical forest	Binary	750	20	10
	Mosaic A, mosaic B and densely forested	3000	5	2
Forest	Mosaic A	1000	20	10
	Mosaic B and densely forested	1500	20	10

Table 2. LULC types and related tree cover implemented in Rockyfor3D. Nb.trees.ha values correspond to the density of trees (number of stems per hectare). Mean diameter of trees and associated standard deviation are described by DBH mean and DBH std values, respectively. Based on these values, the Rockyfor3D model randomly placed a given number of trees within each of the covered allotments (Dorren, 2012).

	Pattern							
	Binary		Mosaic A		Mosaic B		Densely forested	
Nb_{TOT} houses reached	342		263		260		177	
$p_z < 0.01\%$	328	(96%)	217	(83%)	244	(94%)	163	(92%)
$0.01\% \leq p_z < 0.05\%$	14	(4%)	27	(10%)	13	(5%)	12	(7%)
$0.05\% \leq p_z < 0.1\%$	0	(0%)	8	(3%)	3	(1%)	1	(0.5%)
$p_z \geq 0.1\%$	0	(0%)	11	(4%)	0	(0%)	1	(0.5%)

Table 3. Descriptive statistics of the number of houses impacted from Rockyfor3D simulations and reported in four reach probability classes (regardless of the volume class) for the four LULC patterns considered.

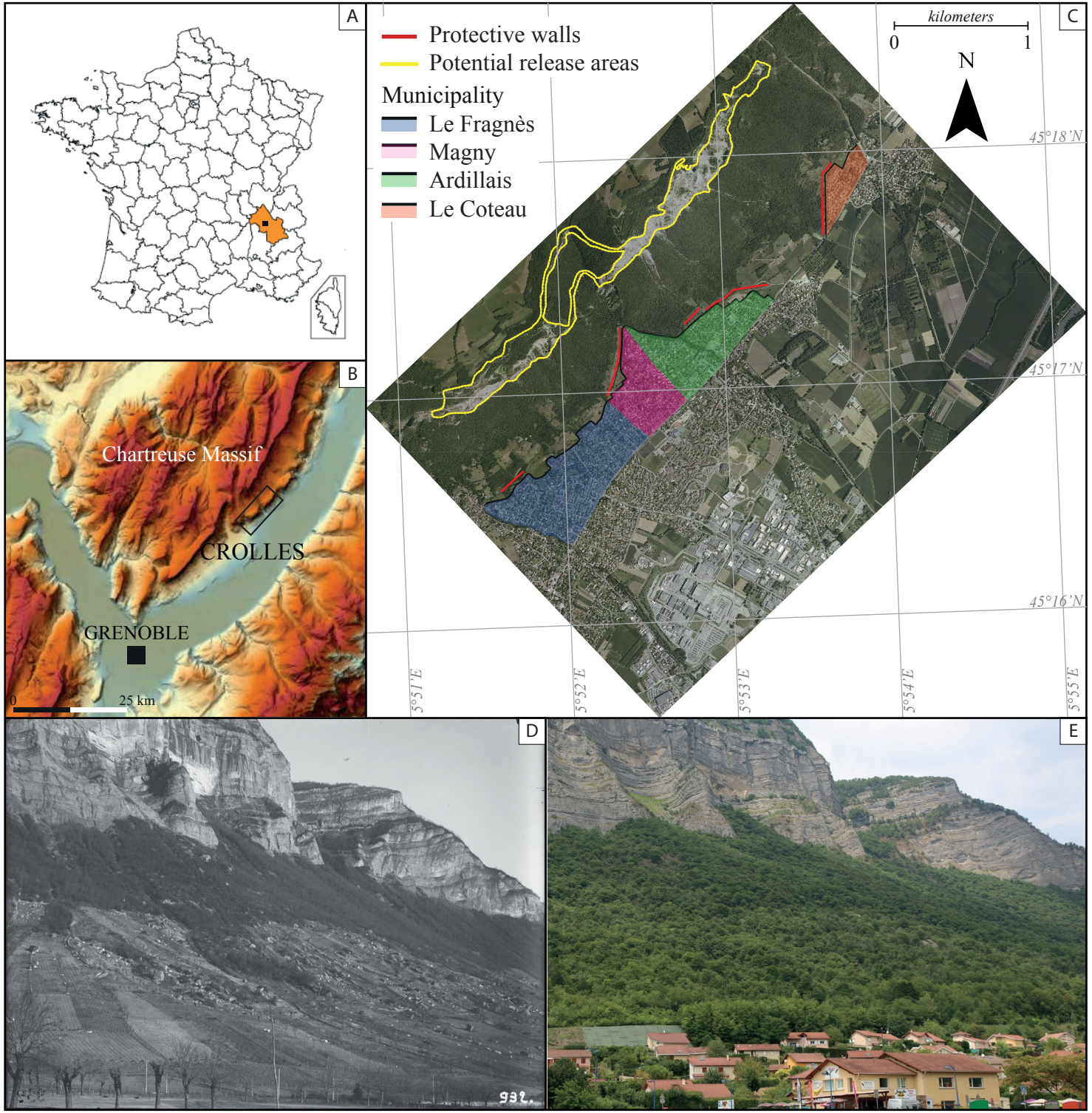
A
B
C
D
E
Protective walls
Potential release areas
Municipality
Le Fragnès
Magny
Ardillais
Le Coteau
kilometers
0
1
N
45°18'N
45°17'N
45°16'N
5°51'E
5°52'E
5°53'E
5°54'E
5°55'E
Chartreuse Massif
CROLLES
GRENOBLE
0
25 km

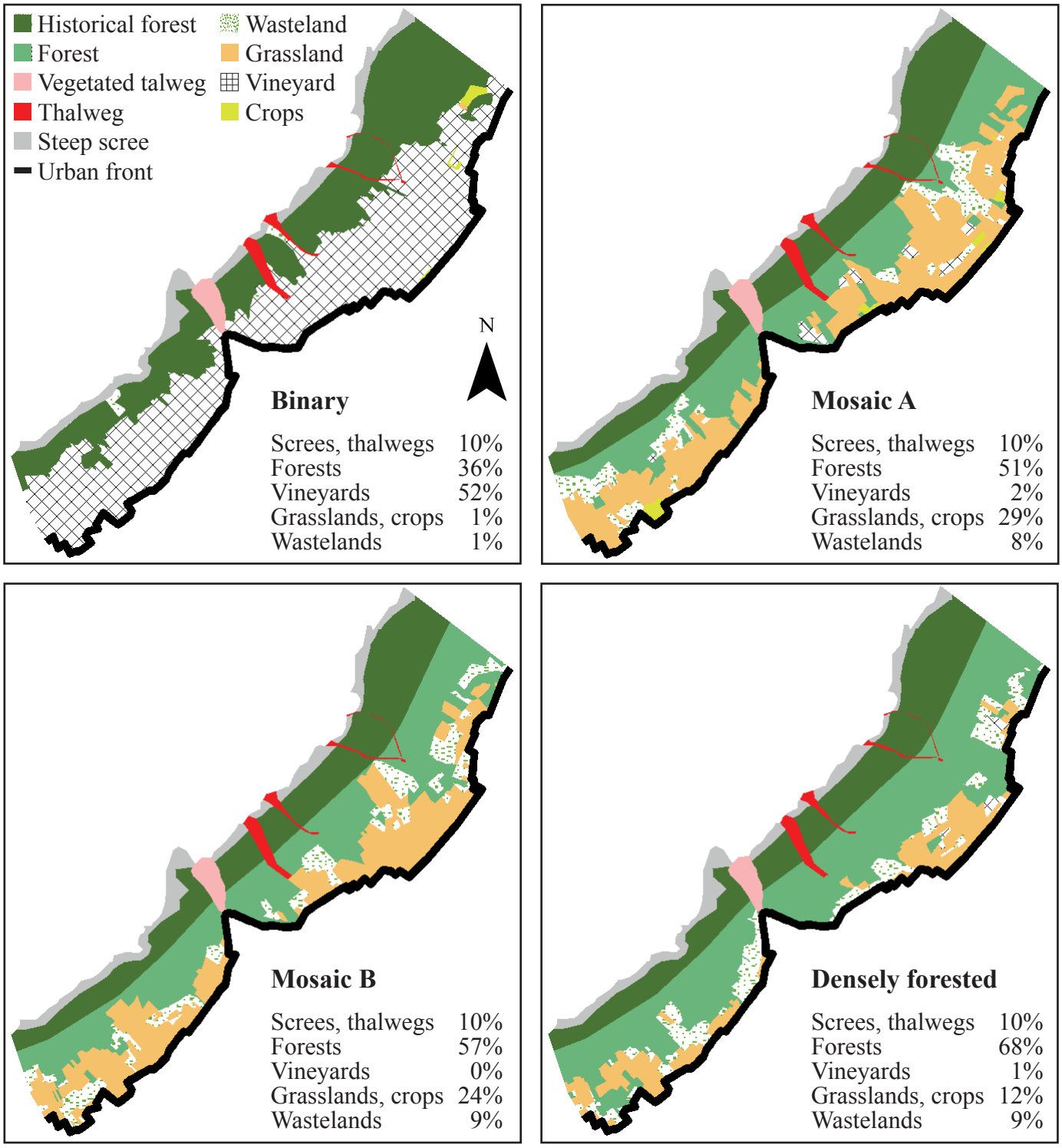
Historical forest
Forest
Vegetated talweg
Thalweg
Steep scree
Urban front
Wasteland
Grassland
Vineyard
Crops
N
Binary
Screes, thalwegs 10%
Forests 36%
Vineyards 52%
Grasslands, crops 1%
Wastelands 1%
Mosaic A
Screes, thalwegs 10%
Forests 51%
Vineyards 2%
Grasslands, crops 29%
Wastelands 8%
Mosaic B
Screes, thalwegs 10%
Forests 57%
Vineyards 0%
Grasslands, crops 24%
Wastelands 9%
Densely forested
Screes, thalwegs 10%
Forests 68%
Vineyards 1%
Grasslands, crops 12%
Wastelands 9%

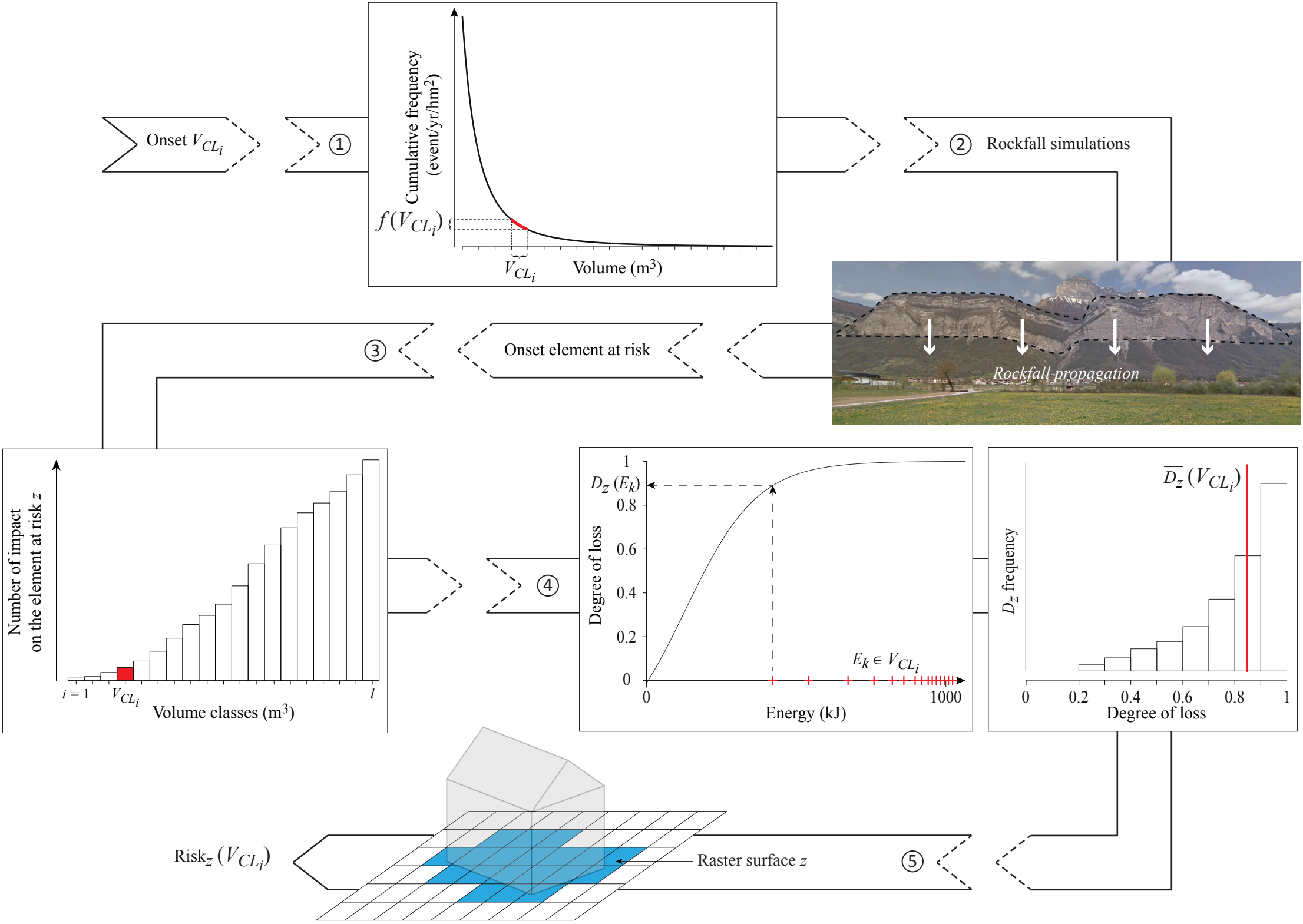
Onset V_{CL_i}
1
Cumulative frequency (event/yr/hm²)
$f(V_{CL_i})$
V_{CL_i}
Volume (m³)
2
Rockfall simulations
Rockfall propagation
3
Onset element at risk
Number of impact on the element at risk z
$i = 1$
V_{CL_i}
l
Volume classes (m³)
4
1
$D_z(E_k)$
0.8
0.6
0.4
0.2
0
Degree of loss
$E_k \in V_{CL_i}$
0
1000
Energy (kJ)
$\overline{D_z}(V_{CL_i})$
D_z frequency
0
0.2
0.4
0.6
0.8
1
Degree of loss
$\text{Risk}_z(V_{CL_i})$
Raster surface z
5

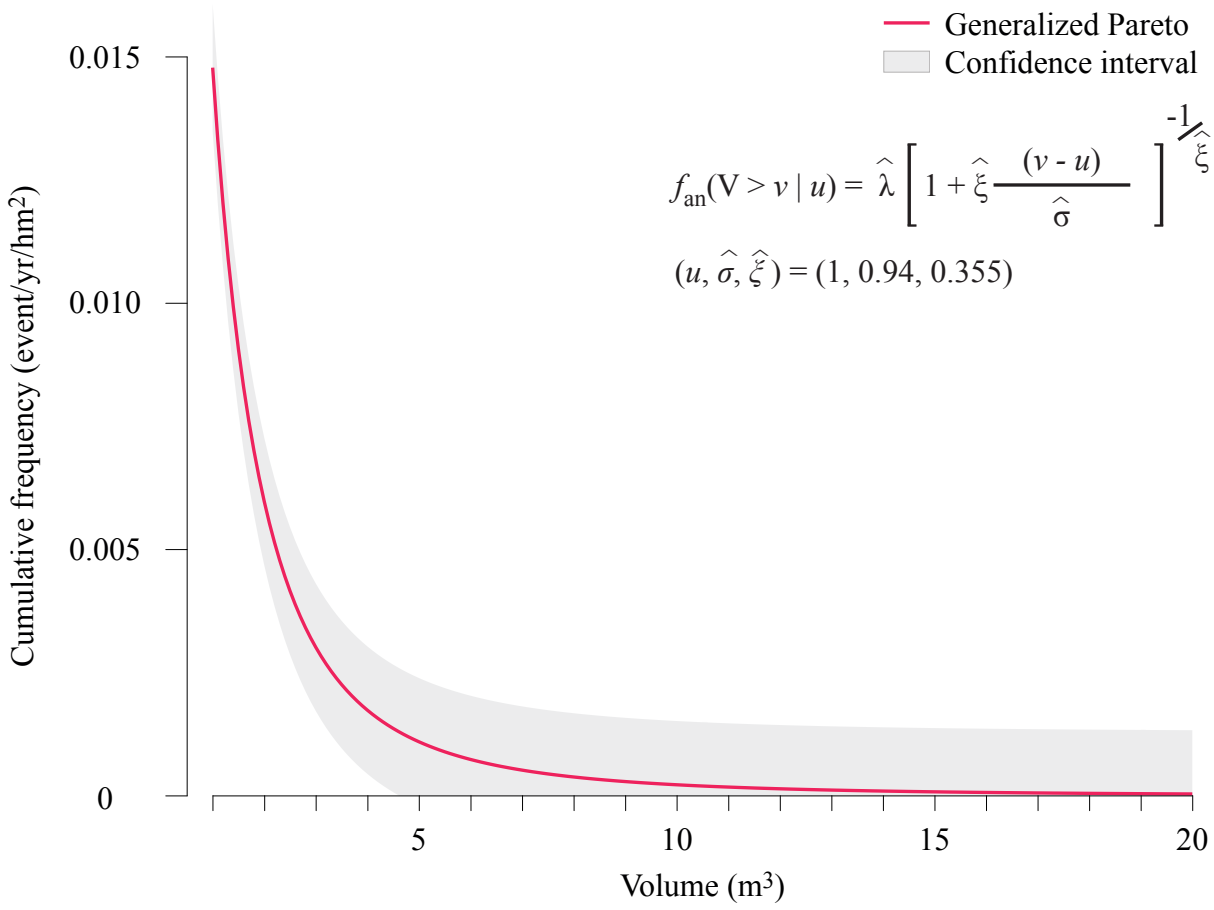
Generalized Pareto
Confidence interval
$f_{an}(V > v \mid u) = \hat{\lambda}\left[1 + \hat{\xi}\frac{(v-u)}{\hat{\sigma}}\right]^{-1/\hat{\xi}}$
$(u, \hat{\sigma}, \hat{\xi}) = (1, 0.94, 0.355)$
Cumulative frequency (event/yr/hm²)
0.015
0.010
0.005
0
5
10
15
20
Volume (m³)

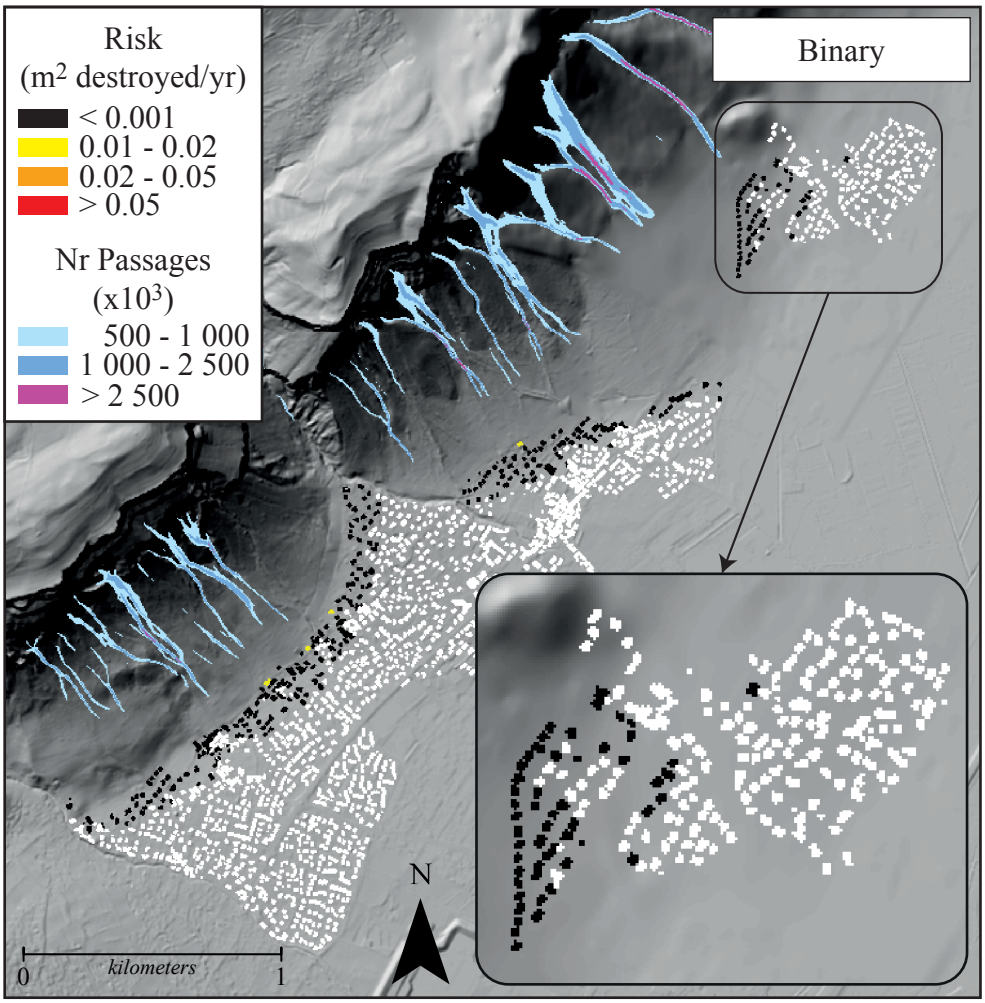
Risk
(m2 destroyed/yr)
< 0.001
0.01 - 0.02
0.02 - 0.05
> 0.05
Nr Passages
(x10³)
500 - 1 000
1 000 - 2 500
> 2 500
Binary
N
0
kilometers
1

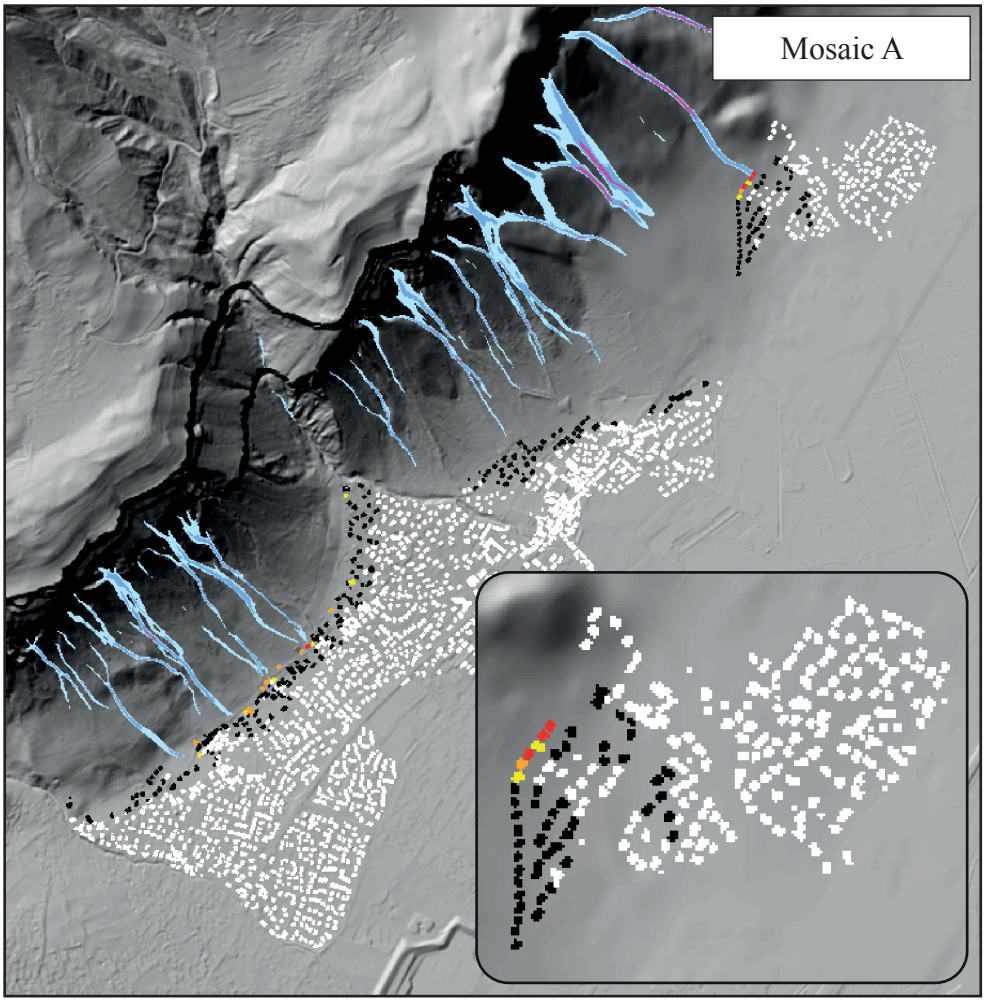
Mosaic A

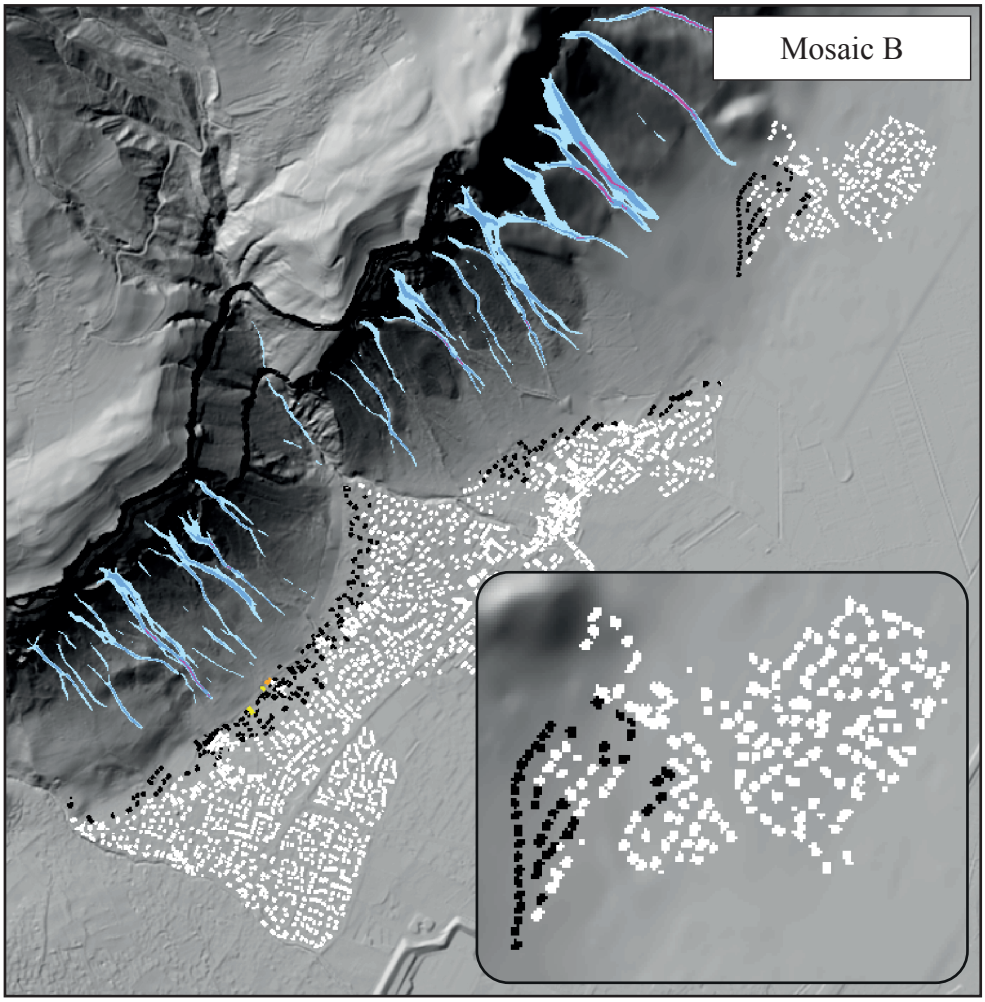
Mosaic B

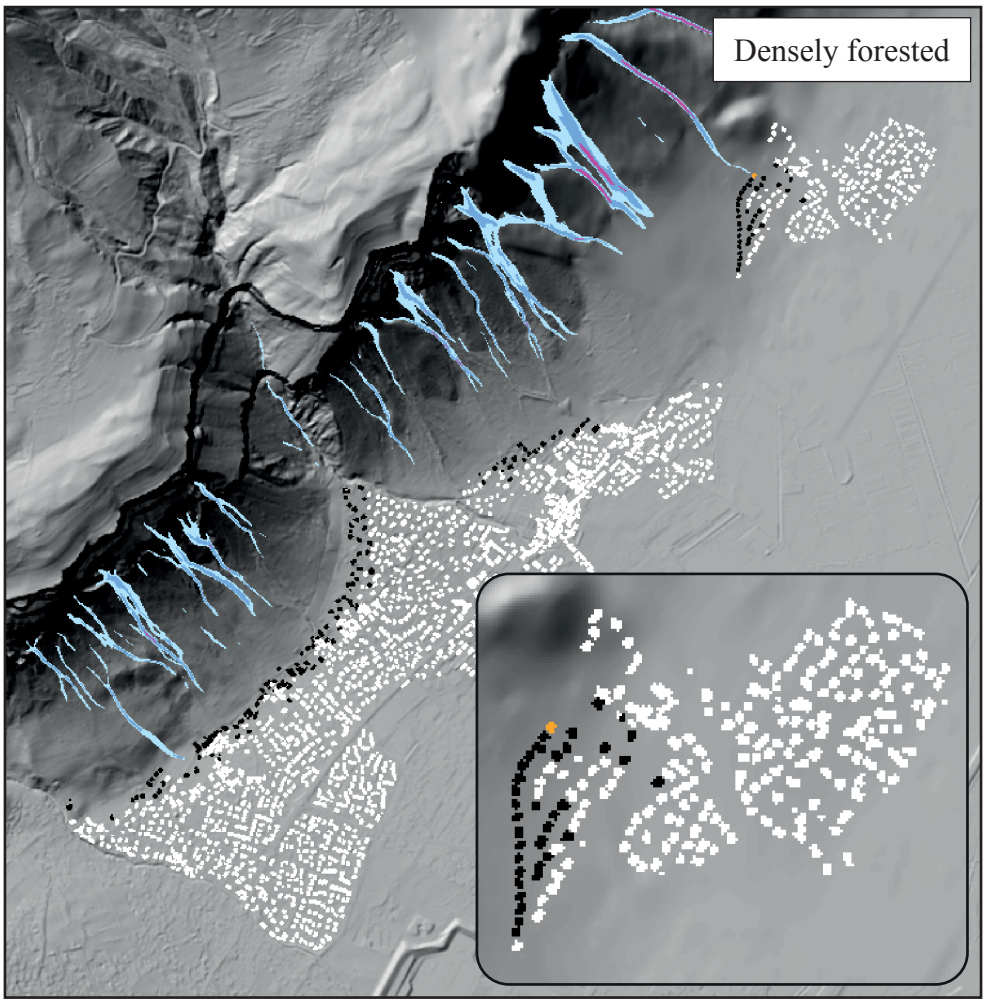
Densely forested

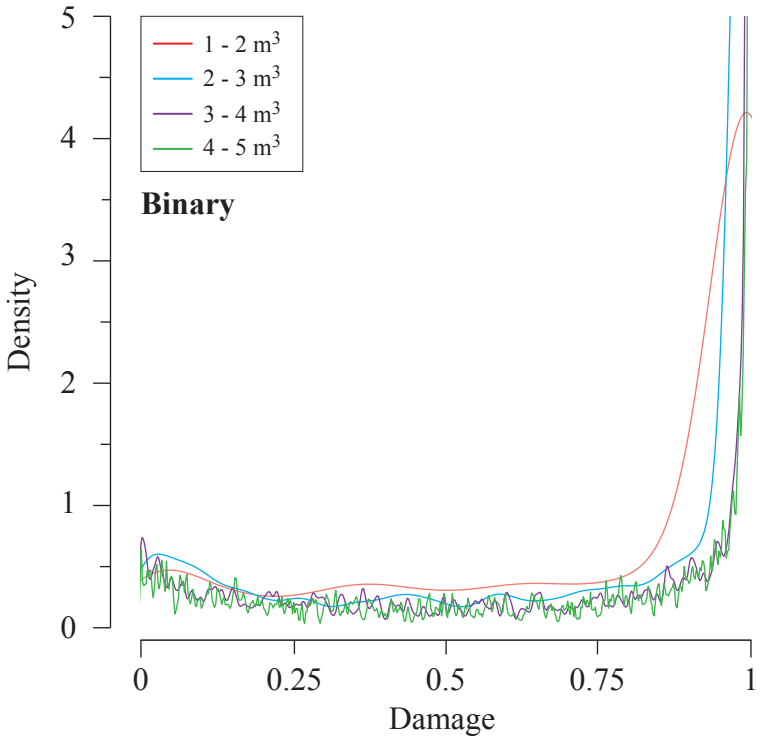
1 - 2 m3
2 - 3 m3
3 - 4 m3
4 - 5 m3
Binary
Density
Damage
0
1
2
3
4
5
0
0.25
0.5
0.75
1

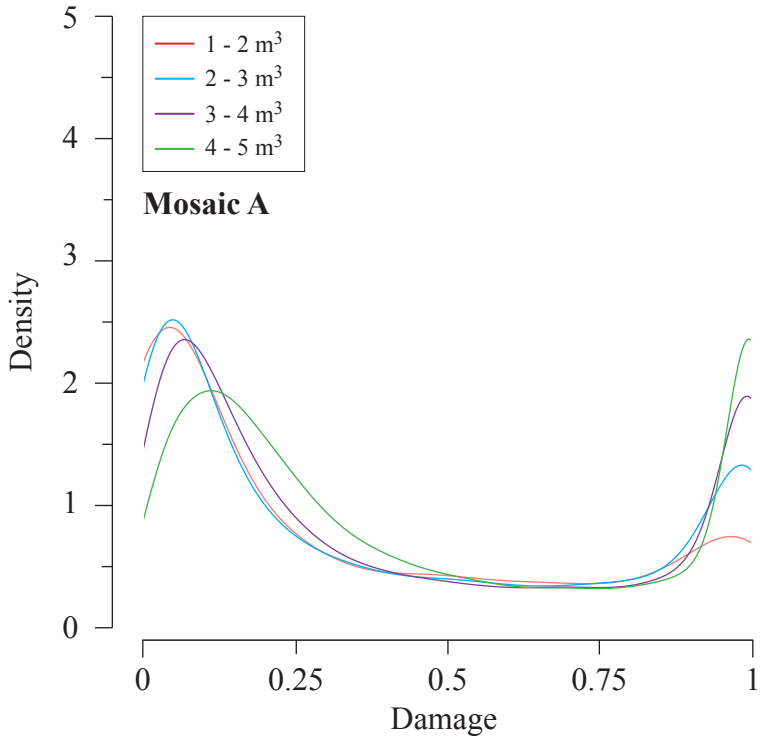
1 - 2 m3
2 - 3 m3
3 - 4 m3
4 - 5 m3
Mosaic A
Density
Damage
0
1
2
3
4
5
0
0.25
0.5
0.75
1

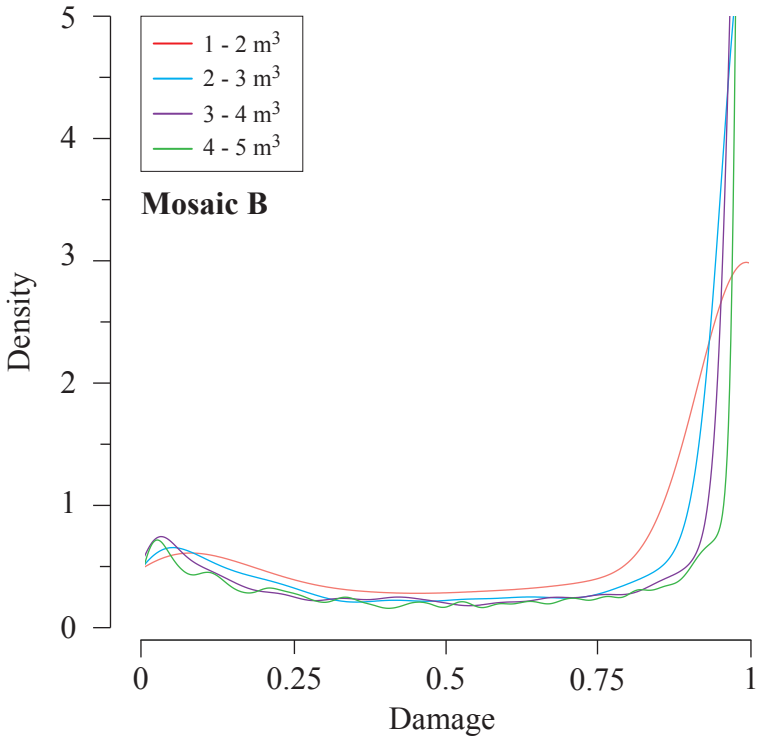
1 - 2 m3
2 - 3 m3
3 - 4 m3
4 - 5 m3
Mosaic B
Density
Damage
0
1
2
3
4
5
0
0.25
0.5
0.75
1

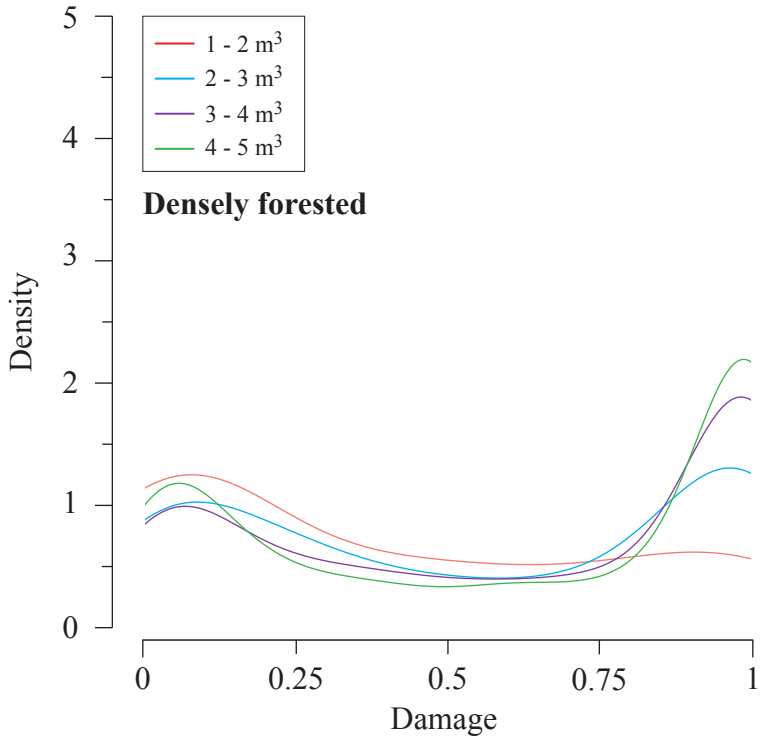
1 - 2 m3
2 - 3 m3
3 - 4 m3
4 - 5 m3
Densely forested
Density
Damage
0
1
2
3
4
5
0
0.25
0.5
0.75
1

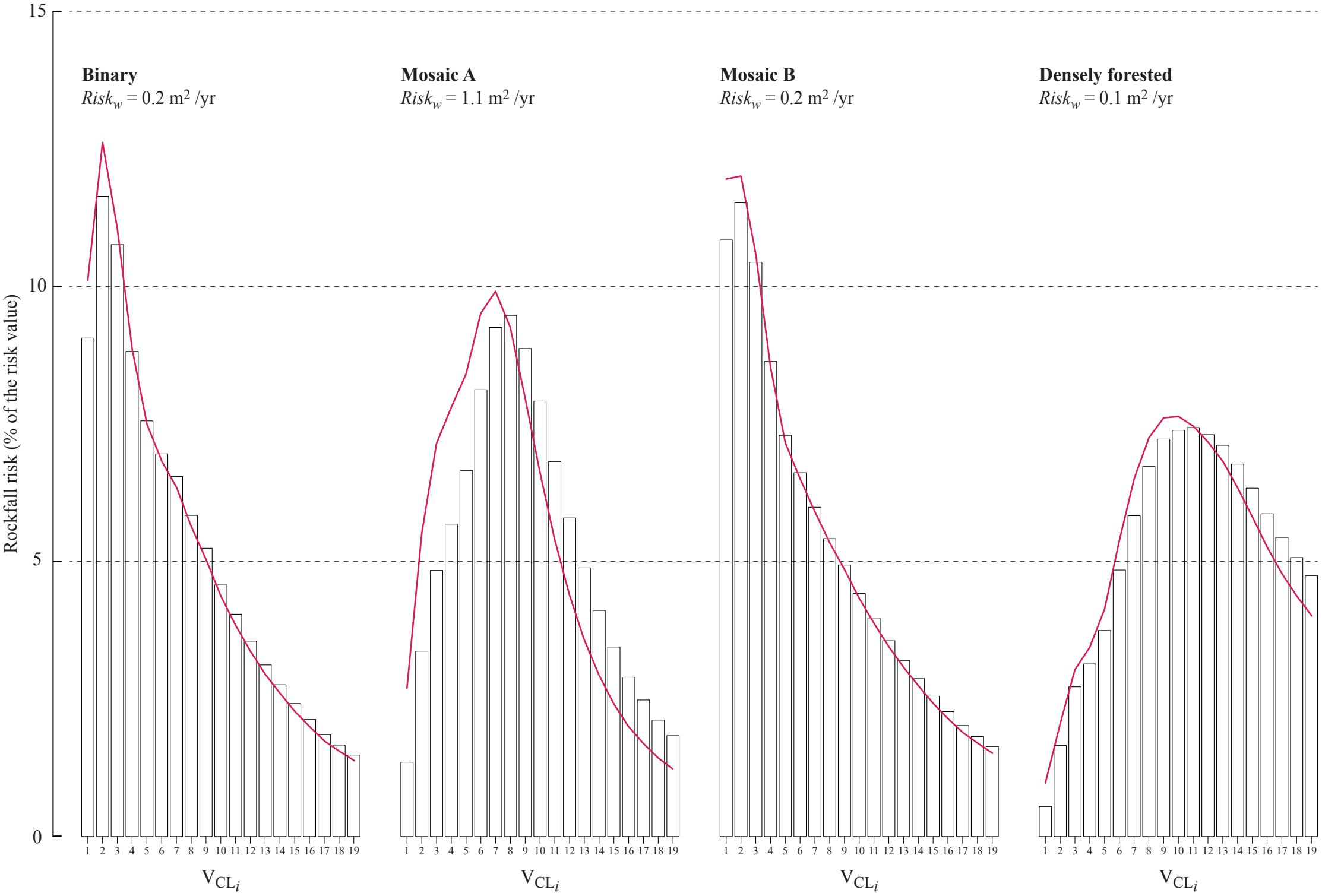
15
10
5
0
Rockfall risk (% of the risk value)
Binary
$Risk_w$ = 0.2 m² /yr
Mosaic A
$Risk_w$ = 1.1 m² /yr
Mosaic B
$Risk_w$ = 0.2 m² /yr
Densely forested
$Risk_w$ = 0.1 m² /yr
1 2 3 4 5 6 7 8 9 10 11 12 13 14 15 16 17 18 19
V_{CL_i}

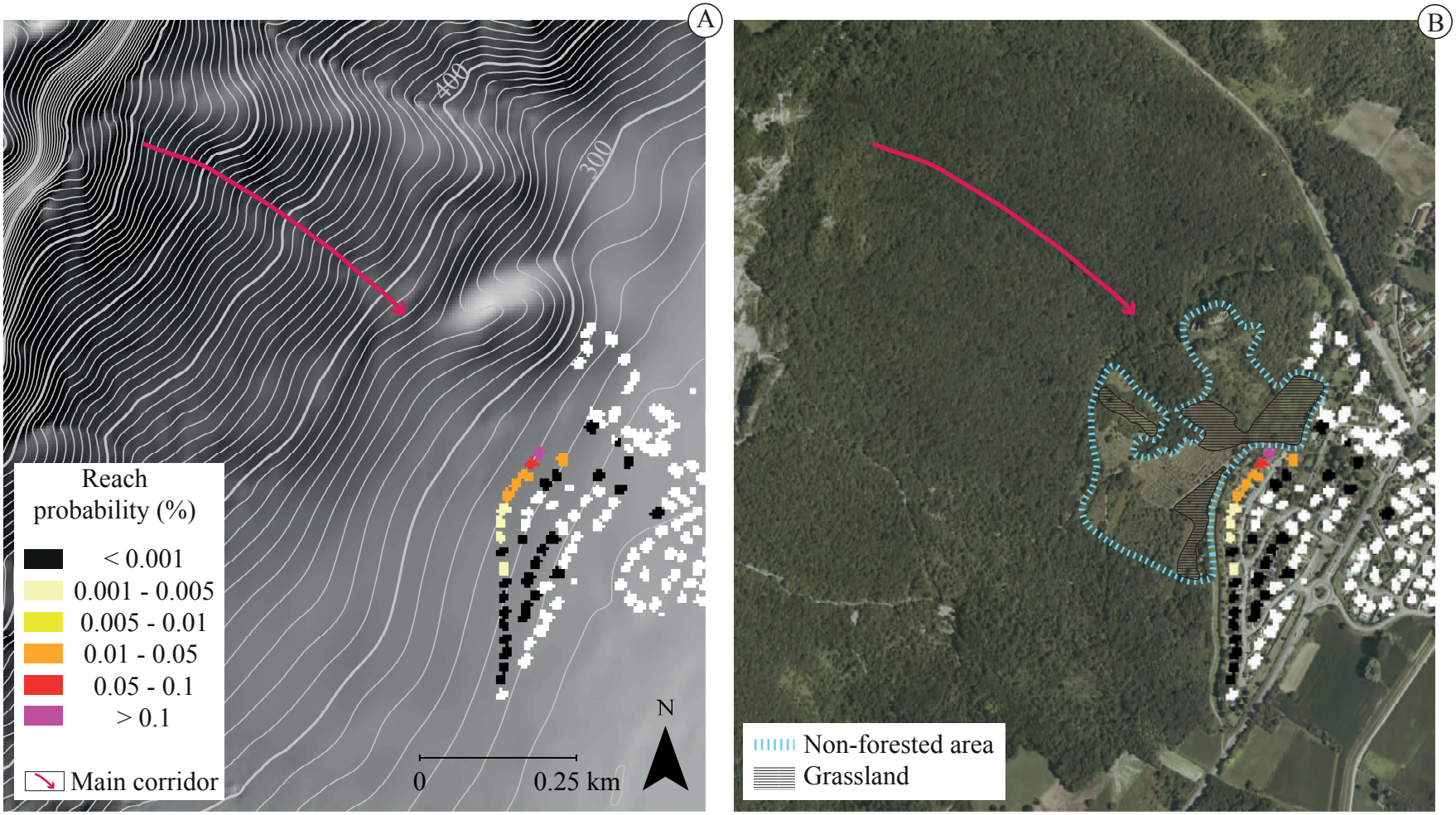
A
400
300
Reach probability (%)
< 0.001
0.001 - 0.005
0.005 - 0.01
0.01 - 0.05
0.05 - 0.1
> 0.1
Main corridor
0
0.25 km
N
B
Non-forested area
Grassland